JACS Au
AN OPEN ACCESS JOURNAL OF THE AMERICAN CHEMICAL SOCIETY

pubs.acs.org/jacsau
Article

Chemical and Redox Noninnocence of Pentane-2,4-dione Bis(*S*-methylisothiosemicarbazone) in Cobalt Complexes and Their Application in Wacker-Type Oxidation

Vincent Porte,[▽] Miljan N. M. Milunovic,[▽] Ulrich Knof, Thomas Leischner, Tobias Danzl, Daniel Kaiser, Tim Gruene, Michal Zalibera, Ingrid Jelemenska, Lukas Bucinsky, Sergio A. V. Jannuzzi, Serena DeBeer,* Ghenadie Novitchi, Nuno Maulide,* and Vladimir B. Arion*

Cite This: *JACS Au* 2024, 4, 1166−1183

Read Online

ACCESS | Metrics & More | Article Recommendations | Supporting Information

ABSTRACT: Cobalt complexes with multiproton- and multielectron-responsive ligands are of interest for challenging catalytic transformations. The chemical and redox noninnocence of pentane-2,4-dione bis(*S*-methylisothiosemicarbazone) (PBIT) in a series of cobalt complexes has been studied by a range of methods, including spectroscopy [UV−vis, NMR, electron paramagnetic resonance (EPR), X-ray absorption spectroscopy (XAS)], cyclic voltammetry, X-ray diffraction, and density functional theory (DFT) calculations. Two complexes $[Co^{III}(H_2L^{SMe})I]I$ and $[Co^{III}(L^{SMe})I_2]$ were found to act as precatalysts in a Wacker-type oxidation of olefins using phenylsilane, the role of which was elucidated through isotopic labeling. Insights into the mechanism of the catalytic transformation as well as the substrate scope of this selective reaction are described, and the essential role of phenylsilane and the noninnocence of PBIT are disclosed. Among the several relevant species characterized was an unprecedented Co(III) complex with a dianionic diradical PBIT ligand ($[Co^{III}(L^{SMe\bullet\bullet})I]$).

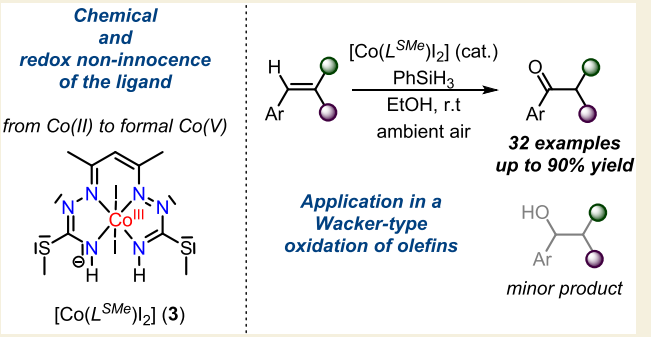

KEYWORDS: *cobalt, pentane-2,4-dione bis(S-methylisothiosemicarbazone), noninnocence, redox, multiproton, ketone, olefin, oxidation*

INTRODUCTION

Metal complexes with redox-active and redox noninnocent ligands[1−7] continue to spark the interest of the chemical community[8−11] as they not only boast intriguing electronic structures,[12−14] as well as spectroscopic[15−17] and magnetochemical properties,[18−21] but also promise new opportunities for catalysis.[22−28] A particular point of interest of redox-active ligands is their ability to act as electron reservoirs, enabling substrate activation at a metal center via intramolecular ligand−metal electron transfer.[3,29] The propensity of redox-active ligands to bring about new reactivity at a bound transition metal and to promote challenging multielectron catalytic transformations by avoiding pathways with high-energy intermediates also motivates their use in catalysis.[23,30] The recent replacement of noble metals (classically undergoing $2e^-$ transformations) by a combination of earth-abundant first-row transition metals and redox-active ligands (both enabling $1e^-$ redox events under mild conditions) in catalytic transformations such as water oxidation is just one prominent example (Scheme 1a).[23,30]

Distribution of the charges over several sites (metals and ligands), avoiding charge accumulation at a single metal center, endows the employed base metal with noble metal character.[3] At the same time, the stability of higher-oxidation-state intermediates can be controlled by the redox-active ligand bound tightly to the metal center.[2,31] Other important roles of redox-active ligands in metal complexes used in catalysis have been disclosed recently as (i) regulation of Lewis acidity/basicity of a transition metal by changing the ligand redox state, (ii) generation of ligand-centered radicals, (iii) substrate activation by the formation of a new ligand−substrate bond through radical reactivity, which might also result in inducing different spin states of the metal, and (iv) metal−ligand bifunctional substrate activation by a combined two-electron transfer.[5,23] In addition, the search for new strategies relying on multiproton-storage ligand platforms, featuring reversible protonation and proton-releasing abilities, and redox activity for cooperative metal−ligand bifunctional substrate activation via proton-coupled electron transfer (PCET)—with the goal of

Received: January 2, 2024
Revised: February 9, 2024
Accepted: February 15, 2024
Published: March 12, 2024

Scheme 1. Use of Early Transition Metals in Combination with Redox-Active Ligands Has Led to a Paradigm Shift

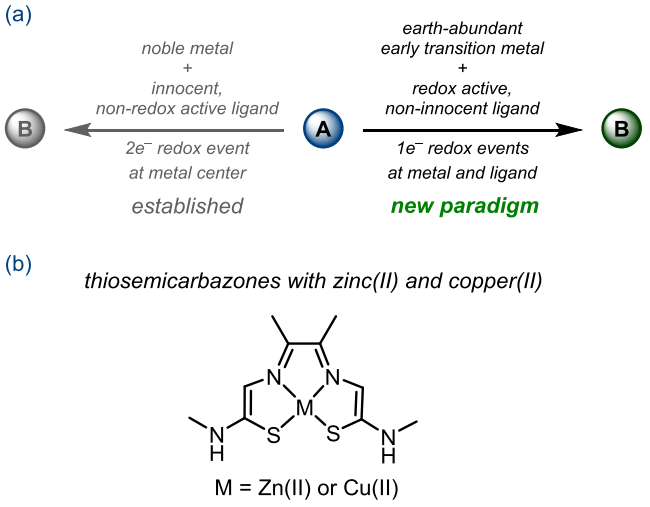

finding new applications in catalysis—has intensified.[5,23,32] This is exemplified by the inclusion of redox and proton-transfer sites into the ligand of a ruthenium catalyst used for water oxidation, which facilitated simultaneous transfer of electrons and protons with a decrease of redox potential, leading to new reaction pathways.[33,34] Of particular note in terms of our interest in coordination chemistry with redox-active (iso)thiosemicarbazones[35] are zinc(II) and copper(II) complexes (Scheme 1b) with a redox-active and proton-responsive tetradentate ligand, namely, diacetyl-bis(*N*-4-methyl-3-thiosemicarbazone), which were reported to catalyze the electrocatalytic hydrogen evolution reaction (HER).[36,37] Cobalt complexes with redox noninnocent ligands have found successful application in a wide variety of catalytic transformations, including Negishi-type C−C cross-coupling reactions,[26] (electro)catalytic C−C bond formation mediated by ligand-centered reduction,[38] and a variety of other C−C and C−heteroatom bond-forming reactions,[17,39−44] among others.[45−48] Multielectron and multiproton catalytic hydrogen evolution reactions with cobalt(II) porphyrin that contains a xanthene moiety with a pendant carboxylic group to assist in proton relay are also well-documented.[49]

The pentane-2,4-dione bis(*S*-methylisothiosemicarbazone) (PBIT) backbone is unique in that it can be coordinated by a metal ion either as fully protonated species H_3L^{SMe}, as monoanion $(H_2L^{SMe})^-$, dianion $(HL^{SMe})^{2-}$, trianion $(L^{SMe})^{3-}$, or as a $2e^-$-oxidized species of the trianion $(L^{SMe})^-$.[35] Although its redox noninnocent behavior has been disclosed in nickel[50] and iron complexes,[51,52] it remains largely unknown for cobalt coordination compounds (Scheme S1).

Ketones are ubiquitous building blocks in man-made chemicals[53] and natural products,[54] and the remarkable breadth of synthetic transformations available to the carbonyl group renders ketones crucial building blocks in organic synthesis.[55] Although a range of classical protocols have been developed to access this key functional handle (e.g., alcohol oxidation, ozonolysis, Weinreb ketone synthesis),[56] ketone syntheses relying on catalytic pathways offer unique benefits related to waste reduction and atom economy.[57] One such well-established, catalytic method for the synthesis of ketones is the Pd-catalyzed Wacker oxidation (Scheme 2a). Initially developed for the conversion of simple ethylene into

Scheme 2. Catalytic Oxidation of Olefins[a]

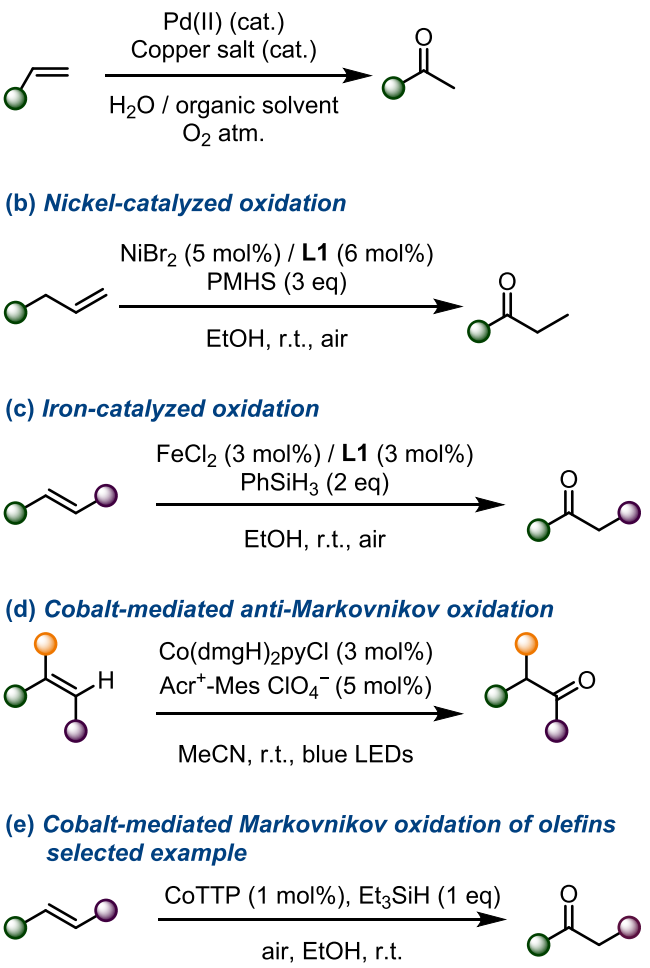

[a](a) Wacker oxidation, (b) nickel-catalyzed oxidation, (c) iron-catalyzed oxidation, (d) cobalt-mediated *anti*-Markovnikov oxidation, (e) cobalt-mediated Markovnikov oxidation. **L1** = 2,9-Dimethyl-1,10-phenanthroline; PMHS = polymethylhydrosiloxane; dmgH = dimethylglyoximate monoanion; py = pyridine; TPP = 5,10,15,20-tetraphenyl-21*H*,23*H*-porphin.

acetaldehyde on an industrial scale (Hoechst−Wacker process), it was further optimized for more general use,[58] typically relying on a Pd(II) catalyst, a redox cocatalyst, and dioxygen as the reoxidant. While Pd and other noble metals have risen to the forefront of this chemistry (see Scheme 1), they present issues of cost and toxicity. The past decade has seen renewed interest in developing earth-abundant base-metal catalysis, with advantages in environmental friendliness and economic viability, of these (and related) oxidations.[59,60] An ideal homogeneous oxidation catalyst is expected to be stable and highly selective, perform well in nontoxic solvents and use air as the sole oxidant.[61] Important contributions in this direction are nickel- and iron-based catalysts to promote the Wacker-type oxidation of olefins (Scheme 2b,c).[62−67] A dual catalytic system involving a cobaloxime and an acridinium photocatalyst that yielded the anti-Markovnikov products under milder conditions was also recently reported (Scheme 2d).[68] With few exceptions (Scheme 2e),[69] previous reports on Co-mediated oxidation of olefins to ketones, in a Markovnikov fashion, either suffer from limitations in scope,[70−74] require

https://doi.org/10.1021/jacsau.4c00005
JACS Au 2024, 4, 1166−1183

harsh conditions,[75] or lead to unspecific reactivity.[76,77] Some works also showed that, in the presence of Co and dioxygen, olefins can undergo oxidative cleavage, rather than oxidative hydration.[78,79]

Herein, we report the synthesis of a series of cobalt complexes supported by a chemically noninnocent and redox noninnocent PBIT ligand (**1**–**3**, Scheme 3), together with

Scheme 3. Conversion of 1 into 2, and 2 into 3

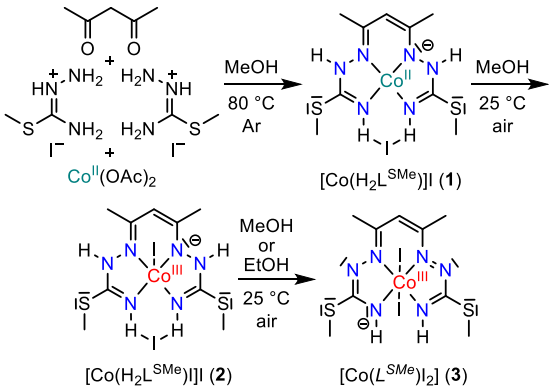

their characterization by NMR, UV–vis, and electron paramagnetic resonance (EPR) spectroscopies, X-ray absorption spectroscopy (XAS), cyclic voltammetry, and spectroelectrochemistry, variable-temperature magnetic-susceptibility measurements, single-crystal and powder X-ray diffraction, and density functional theory (DFT) calculations. We also describe the catalytic activity of these complexes, which, in the presence of a silane and dioxygen—in contrast to the related Mukaiyama hydration, which produces alcohols (Scheme 4a)—chemoselectively transforms olefins into the corresponding ketones in a Wacker-type process (Scheme 4b).

Scheme 4. (a) Mukaiyama Hydration and (b) Wacker-Type Oxidation

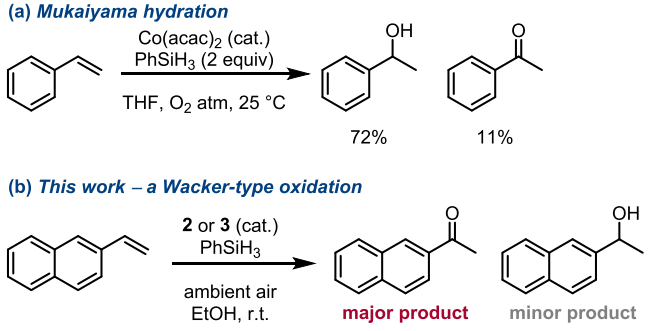

We also present mechanistic studies highlighting the essential role of phenylsilane and the noninnocence of the PBIT platform to enable this new catalytic oxidation of olefins.

RESULTS AND DISCUSSION

Synthesis and Characterization of Cobalt Complexes in Various Protonation and Oxidation States

Our studies began with the synthesis of [Co(H_2L^{SMe})]I (**1**, see Scheme 3 and Section S1) through condensation of pentane-2,4-dione (Hacac) with *S*-methylisothiosemicarbazidium iodide in the presence of cobalt(II) acetate. Reaction in methanol, heating at 80 °C under inert atmosphere, afforded a brown-cherry crystalline product upon slow cooling. The structure of the square-planar cobalt(II) complex [Co(H_2L^{SMe})]I·0.5CH_3OH (**1·0.5CH$_3$OH**),[80] in which the tetradentate ligand acts as a monoanion $(H_2L^{SMe})^-$, was established by single-crystal X-ray diffraction (SC-XRD) (vide infra, Figure 1).

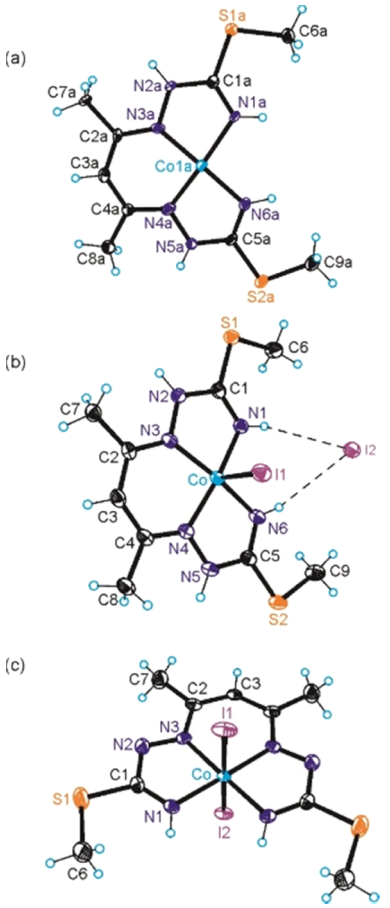

Figure 1. Oak ridge thermal-ellipsoid plot program (ORTEP) views of complex cations in (a) **1·0.5CH$_3$OH** and complexes (b) **2·CH$_3$OH** and (c) **3** with atom labeling schemes. Thermal ellipsoids are drawn at 50% probability level.

Notably, exposure of a solution of **1** to air resulted in gradual oxidation, as indicated by a striking color change of the brown-cherry solution to green-blue. The resulting solution, when left in a closed flask, produced blue-black crystals of [Co^{III}(H_2L^{SMe})I]I·CH_3OH (**2·CH$_3$OH**), the structure of which was determined by SC-XRD (see Sections S1–S4 for detailed characterization).[81] Recrystallization of five-coordinate [Co^{III}(H_2L^{SMe})I]I (**2**) from ethanol or methanol in the presence of air afforded a six-coordinate complex, formulated as [Co^{III}(L^{SMe})I_2] (**3**) (see Scheme 5), through a 2e$^-$ oxidation followed by the release of two protons. The central atom preserves its oxidation state +3 (rather than +5; see in-depth characterization below and in Sections S1–S3), where the fully deprotonated ligand is a two-electron-oxidized 12π-electron monoanion, which is denoted herein in italic style as $(L^{SMe})^-$, to contrast it to the 14π electronic species $(L^{SMe})^{3-}$ of the putative Co^V complex [Co^V(L^{SMe})I_2] (Scheme 5, right), in

https://doi.org/10.1021/jacsau.4c00005
JACS Au 2024, 4, 1166–1183

Scheme 5. Ambiguity in the Assignment of the Oxidation Level of PBIT and Co in 3

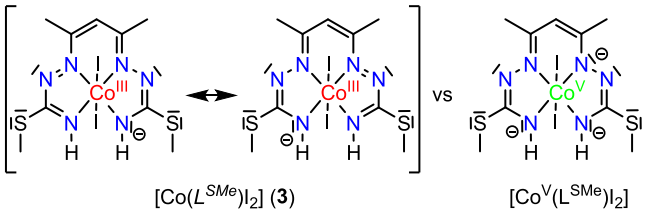

which the tetradentate ligand is fully deprotonated ($(L^{SMe})^{3-}$), and two iodido coligands are bound axially.[82]

To find out whether other coordination geometries and/or protonation levels of the PBIT ligand in cobalt complexes can be reached, we performed a set of reactions with reductants and oxidants.

Other Cobalt(III) Complexes

Air exposure of an ethanolic solution of **1** produced dark-red crystals of the dimeric associate $[Co^{III}(L^{SMe,O})I]_2 \cdot C_2H_5OH$ (**4·C_2H_5OH**, see Section S1), in which each monoanionic ligand is oxidized at the central carbon of the Hacac moiety with the formation of a keto group $H_2L^{SMe,O}$ = 3-oxo-pentane-2,4-dione bis(*S*-methylisothiosemicarbazone), a reaction typical for transition-metal complexes with pentane-2,4-dione bis(thiosemicarbazones).[83−85] The dimeric structure was disclosed by SC-XRD and IR spectroscopy (see Sections S1 and S2).

The reduction of complex **2** with phenylsilane under inert conditions and the consecutive exposure to air yielded mononuclear $[Co^{III}(L^{SMe,O})I(CH_3OH)]$ (**5**, see Sections S1 and S2 for details).

Other Cobalt(II) Complexes

In addition, it was found that the reaction of complex **2** in the presence of $PhSiH_3$ under inert conditions afforded six-coordinate cobalt(II) complex $[Co^{II}(H_3L^{SMe})I(CH_3OH)]I \cdot CH_3OH$ (**6·CH_3OH**), where the PBIT ligand preserved its fully protonated form (a similar behavior was observed in other cobalt(II) complexes, see Sections S1 and S2).

High-resolution X-ray crystallography allows for reliable assignment of the oxidation state of the redox-active or redox noninnocent ligand via comparison of bond metrics in similar compounds available in the literature,[86] while the oxidation state of the central metal ion can be established by X-ray absorption spectroscopy,[87] even if the ligand is a radical.[88] Both tools have been successfully applied herein to resolve the ambiguity in the assignment of oxidation states of both PBIT and cobalt.

X-ray Crystallographic Investigations of 1−3

In order to facilitate structural comparison of the cobalt complexes with different levels of protonation of PBIT and different oxidation states of both the ligand and metal, single crystals of **1·0.5CH_3OH**, **2·CH_3OH** and **3** were subjected to SC-XRD investigations (see Section S2 for data collection, refinement, and metrical parameters, also for the other cobalt(II) and cobalt(III) complexes).

The coordination geometry of the Co^{II} ion (d^7) in **1·0.5CH_3OH** was found to be square-planar (Figure 1a). While, in the solid state, the vast majority of cobalt(II) complexes are distorted five- or six-coordinate species,[89−94] square-planar cobalt(II) complexes have also been reported.[95−99]

The complex **2·CH_3OH** is square-pyramidal (Figure 1b), with the monoanionic ligand $(H_2L^{SMe})^-$ coordinated to cobalt(III) in the basal plane and one iodido coligand in apical position. The second iodide acts as a counteranion and as a proton acceptor to two end NH groups in the plane of the tetradentate ligand. In addition, one methanol molecule is present in the asymmetric unit. The cobalt-to-apical iodido coligand bond distance of 2.5285(4) Å is well-comparable to that in a similar, previously reported cobalt complex[100] but markedly shorter than that in coenzyme B_{12} model cobaloxime at 2.697(2) Å.[101]

In contrast to five-coordinate complex **2**, complex **3** is six-coordinate with the fully deprotonated tetradentate ligand coordinated equatorially to the central metal ion, while two iodido coligands are bound axially (Figure 1c). As expected, due to increased electronic repulsion in accord with the VSEPR theory, the bond lengths Co−N1, Co−N3, Co−I1, and Co−I2 in this six-coordinate complex are markedly longer than the corresponding bonds in the five-coordinate complex **2**. Given the full deprotonation of the original ligand by loss of three protons and binding of two iodido coligands to the central atom, its formal oxidation state should be +5 (see Scheme 5). As an alternative option, we analyzed the situation where the 14π trianionic ligand $(L^{SMe})^{3-}$ is oxidized by loss of $2e^-$ to give a new 12π monoanionic system $(L^{SMe})^-$. The sum of the bond distances Σ[6(C−N) + 2(N−N) + 2(C−C)] comes to 13.556 Å for $[Co^{III}(H_2L^{SMe})I]I$ and is well-comparable with those in $[Fe^{IV}(L^{SMe})I]$,[51] its *S*-ethyl derivative,[52] and $[\{Fe^{IV}(L^{SMe})\}_2(\mu\text{-}O)]$[102] at 13.503, 13.491, and 13.495 Å, respectively. For $[Co(L^{SMe})I_2]$, in contrast, this sum is clearly smaller of 13.468 Å and is almost identical with the average value for two crystallographically independent anions in $AsPh_4[Fe^{II}(L^{SMe})(CN)_2]$[52] of 13.470 Å. Thus, inspection of SC-XRD metrical parameters provides strong evidence for physical oxidation states −1 for the tetradentate ligand[103] and +3 for Co in the six-coordinate di-iodido complex **3**.

The electronic structures of catalytically relevant complexes **1**−**3** were further investigated by X-ray absorption spectroscopy (XAS).

X-ray Absorption Spectroscopy

The Co K-edge XAS of $[Co^{II}(H_2L^{SMe})]I$ (**1**), $[Co^{III}(H_2L^{SMe})I]I$ (**2**), and $[Co^{III}(L^{SMe})I_2]$ (**3**) were measured and compared to those of Co^{II} and Co^{III} tris-2,2′-bipyridine complexes $[Co^{II}(bpy)_3]Cl_2$ and $[Co^{III}(bpy)_3]Cl_3$ as reference (Figure 2a). As the oxidation state decreases, the lower effective nuclear charge further destabilizes the Co 1s electron, decreasing the energy required to remove it. This effect is evident in the pair of tris-bipyridine reference compounds in the rising edge region at 7717−7725 eV, as the rising edge of the Co^{II} complex is shifted to lower energies. The complexes **1**−**3** show the rising edge region at 7714−7717 eV shifted to even lower energies than $[Co^{II}(bpy)_3]Cl_2$ as a result of the larger covalency of the metal−ligand bonds with the PBIT ligand relative to bipyridine and not due to the lower oxidation state. The effect of covalency on the position of the K-edge is known and is nicely illustrated by the ferric halide series.[104] Despite both **2** and **3** being trivalent and the PBIT ligands both being monoanionic, the rising edge of the former is shifted to lower energies relative to the latter. The $(H_2L^{SMe})^-$ ligand in **2**

https://doi.org/10.1021/jacsau.4c00005
JACS Au 2024, 4, 1166−1183

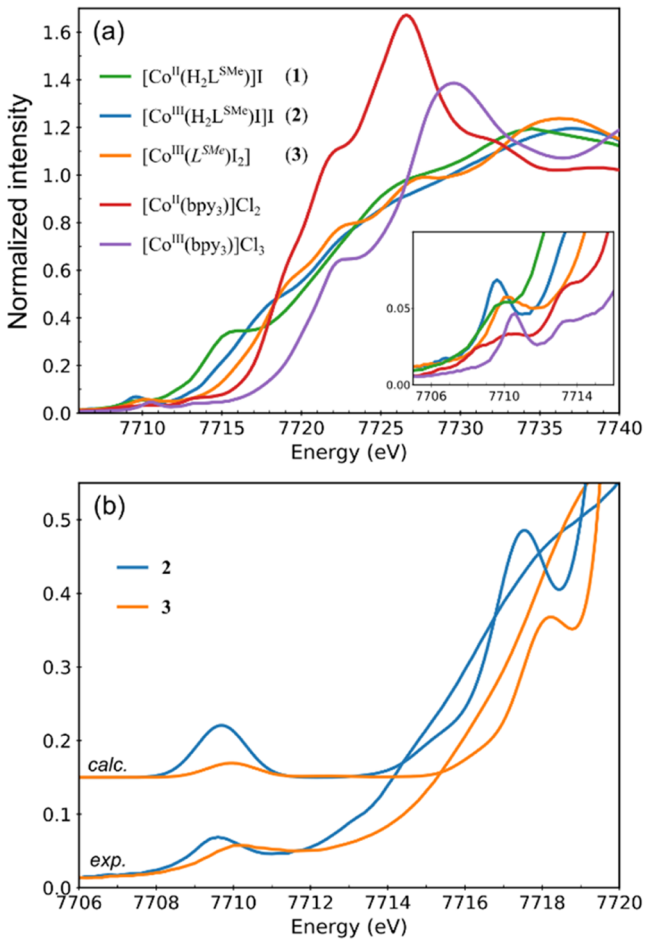

Figure 2. (a) Co K-edge XAS of **1**−**3**, $[Co^{II}(bpy)_3]Cl_2$, $[Co^{III}(bpy)_3]Cl_3$, and expanded pre-edge region (inset). (b) Overlay of the experimental spectra of $[Co^{III}(H_2L^{SMe})I]I$ (**2**) and $[Co(L^{SMe})I_2]$ (**3**) with the respective calculated spectra by time-dependent density functional theory (TDDFT)/B3LYP (energy shift: 93.3 eV, scaling factor: 0.1, line shape: Gaussian, line width: 1.5 eV).

is the two-proton two-electron reduced equivalent with respect to $(L^{SMe})^-$ in **3**, which is associated with Co−N bonds ca. 0.02 Å shorter and hence more covalent (**2**: 1.860/1.881 Å and **3**: 1.876/1.899 Å). This finding evidences the effect of the ligand oxidation state in the modulation of the metal−ligand bond covalency. A closer inspection revealed that **2** has inflection points at 7713.0 and 7715.9 eV, whereas in **3** these occur at 7714.6 and 7717.4 eV. These features should be associated with the differences in the ligand-based low-lying empty molecular orbitals. Finally, the rising edge of **1** is marked by a distinctive intense feature at 7715 eV, usually associated with the transition to Co $4p_z$, which is low-lying due to the square-planar geometry.[105]

The pre-edge peaks of the PBIT-based complexes **1** and **3** are weaker than for **2**, as expected from the centrosymmetric Co site revealed by X-ray crystallography (see Figure 2 and Section S3 for detailed discussion).[106] The calculated XAS spectra in Figure 2b correctly capture the weaker pre-edge of **3**, its pre-edge peak and rising edge both shifted to higher energies relative to **2**, and the overall number of features. These findings lend credence to the interpretation of the excited states in the pre-edge region under the TDDFT framework.[107−112] The key excited states are assigned in Figure S8 in Section S3.[113] The weak single-featured pre-edge peak of the six-coordinate **3** at 7710.2 eV is associated with two nearly degenerate quadrupole-allowed transitions into the empty d_{z^2} and $d_{x^2-y^2}$. The ground-state electronic configuration is $d_{xz}^2\, d_{yz}^2\, d_{xy}^2\, d_{z^2}^0\, d_{x^2-y^2}^0$ with the d_{z^2} lower than the $d_{x^2-y^2}$ due to the weaker field imposed by the axial *trans*-di-iodido ligands. The relatively stronger single-featured pre-edge peak of the five-coordinate **2** at 7709.6 eV is dominated by the transition into the d_{z^2} admixed with Co $4p_z$. The electronic configuration and d-orbital splitting are similar, with the main difference being that d_{z^2} is stabilized in **2** relative to **3** due to the presence of one apical ligand in **2** instead of two in **3**. This is consistent with the fact that the experimental pre-edge peak of **2** is shifted by 0.6 eV to lower energy relative to **3**.

Finally, the absorption features at the onset of the rising edge at 7715−7716 eV (Figure 2) in both compounds are attributed to transitions into π^* with main C═N within the isothiosemicarbazone moiety (see Figure S8 in Section S3) and the prominent features at 7717−7718 eV are assigned to transitions into a π^* on the three central carbons of the Hacac moiety. The first feature is 1.1 eV higher in **3**, relative to **2**, whereas the second feature is only 0.5 eV higher. This indicates that the oxidation state of the ligand affects mainly the π system located on C═N and offers an explanation why the rising edge of **3** appears more oxidized than **2**. Beyond these two features, the rising edge of **3** displays two more distinct intensity modulations at 7722.5 and 7727.5 eV. According to TDDFT, they are excitations to high-lying MOs with large Co $4p_z$ character combined with the *trans* iodido ligands.

Magnetism and EPR Spectroscopy

Given the purity of the bulk sample (see Section S4, Figure S14), variable-temperature magnetic-susceptibility measurements for complex **1** were performed, attesting low-spin electronic configuration (S = 1/2 ground state, d^7) for cobalt(II) (see Section S4, Figures S15 and S16). The X-band EPR spectroscopy of powdered sample **1** additionally confirmed the antiferromagnetic coupling in the cofacial cation dimers revealed in the magnetic measurements (see Section S4, Figure S17 for details). Together, this evidence further corroborated the proposed structure for **1**.

Kinetics of Oxidation of 2 with Air Oxygen

The kinetics of the oxidation of **2** with air oxygen were studied in EtOH at 20 °C. UV−vis−NIR spectra were recorded over 23 h in an open optical cell and are shown in Figure 3. The evolution of optical bands indicated a consecutive reaction pathway with a relatively stable intermediate. Assuming the oxygen in the solution is in a significant excess to the studied complex, the kinetic traces (Figure 3b) were fit with a simple model involving two consecutive reactions obeying pseudo-first-order kinetics (eq 1).

$$\mathbf{A} \xrightarrow{k_1} \mathbf{B} \xrightarrow{k_2} \mathbf{C} \qquad (1)$$

The global analysis approach with this simplified model reproduced the observed kinetics reasonably well, with the individual rate constants $k_1 = 3.72 \pm 0.07 \times 10^{-4}$ s^{-1} and $k_2 = 2.00 \pm 0.07 \times 10^{-5}$ s^{-1}. The spectra of the three reaction components **A**, **B**, and **C** and the corresponding concentration profiles are shown in Figure 3c,d, respectively. Comparison of the spectra obtained from the kinetic model (Figure 3c, dotted lines) with the spectra of **2**, **3**, and **4** (Figure 3c, solid lines) gained with the authentic samples under Ar atmosphere revealed a very good match. Thus, the oxidation of **2** in EtOH with air oxygen proceeds as a consecutive two-step process

https://doi.org/10.1021/jacsau.4c00005
JACS Au 2024, 4, 1166−1183

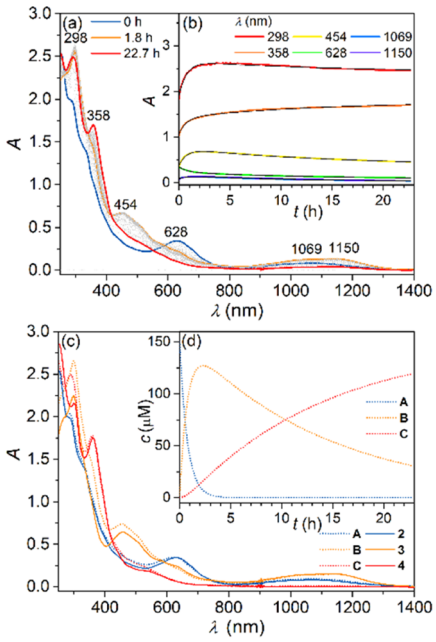

Figure 3. (a) UV−vis−NIR spectra of 150 μM **2** in EtOH oxidized by air oxygen over 23 h; (b) kinetic traces at selected absorption maxima together with the kinetic model fit (see above); (c) dotted lines UV−vis−NIR spectra obtained for the three compounds **A**, **B**, and **C** used in the kinetic model, solid lines UV−vis−NIR spectra of 150 μM **2**, **3** and 75 μM **4** in EtOH under Ar; (d) concentration profiles for the three compounds **A**, **B**, and **C** from the kinetic model.

with the six-coordinate complex **3** as an intermediate, and complex **4** as the final product.

Electrochemical and Spectroelectrochemical Studies

Electrochemical investigation of complexes **1** and **2** (with PBIT ligand in $(H_2L^{SMe})^-$ form), **3** (with $(L^{SMe})^-$ ligand), **4** (with $(L^{SMe,O})^{2-}$ ligand), and **8** (with $(H_3L^{SMe})^0$ ligand) was carried out by cyclic voltammetry (Figure 4 and Section S5, Figure S18).

Half-wave potentials $E_{1/2}$ for electrochemically reversible processes and cathodic peak potentials E_{pc} for electrochemically irreversible events for **1**−**3** (Figure 4), **4**, and **8** were measured (see Section S5 for detailed graphical representation; Table S6 and Figure S18). In the investigated potential window, the Co^{II} complex **1** features a reversible single-electron oxidation at $E_{1/2}$ = −0.39 V vs Fc^+/Fc and three irreversible reductions with E_{pc} of −1.36, −1.89, and −2.56 V, respectively. An essentially identical voltammetric record was obtained with Co^{III} complex **2**, where in turn the redox event at $E_{1/2}$ = −0.40 V represents the first single-electron reduction of the compound. Complex **3** displays a rather complex cathodic response comprising three irreversible reductions at E_{pc} of −0.45, −1.43, and −2.67 V vs Fc^+/Fc, respectively. Complexes **1** and **2** bear the same PBIT ligand, but differ by charge state and the formal oxidation state of the central metal. The reversible redox process found in their CV records at ca. −0.40 V can thus be assigned to the redox transformation of the central metal representing the Co^{III}/Co^{II} redox couple (in **1** Co^{II} is oxidized to Co^{III}, in **2** Co^{III} is reduced to Co^{II}, vide supra). The assignment is corroborated by spectroelectrochemical analysis (Figure 5a,c).

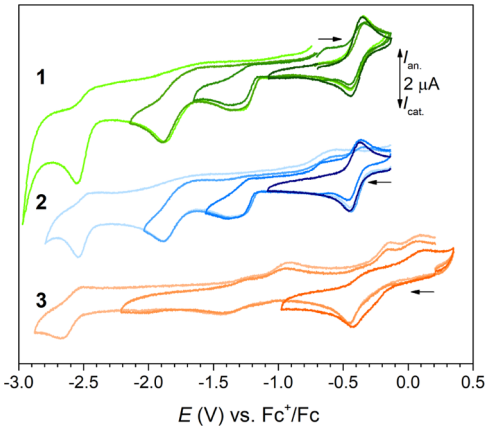

Figure 4. Cyclic voltammograms of ∼0.5 mM **1**−**3** in 0.1 M nBu$_4$NPF$_6$/MeCN, recorded with glassy carbon working electrode at a scan rate of 0.1 V s^{-1}. Scans with different vertex potentials examining the reversibility of individual redox processes are shown with varying color tone. Horizontal arrows indicate the CV scan direction.

Single-electron oxidation of **1** provides UV−vis−NIR spectra identical to those of complex **2** in nBu$_4$NPF$_6$/MeCN, where the blue-green color of the solution is caused by characteristic absorption at 644 nm and the NIR band at 1063 nm also appears. Vice versa, the optical spectra obtained upon the first reduction of **2** almost lack the absorption in the visible range and match the bands of complex **1**.

The reduction of complex **3** at E_{pc} of −0.45 V is electrochemically irreversible, and repeated CV scans (not shown) reveal a successive decrease in cathodic peak current, indicating a follow-up chemical reaction. Therefore, the Co^{II} complex obtained from **3** is unstable and undergoes an as of yet unidentified transformation in solution.

Additional reductions were observed in the entire complex series at potentials more negative than −1.5 V. We believe these to be reductions of the PBIT ligand (see Section S5 for details).

Computational Studies of Complexes 1−3

Evaluation of the metrical charge of the ligands (oxidation level of the ligand,[114] metrical oxidation state)[115] was performed following previously reported approaches.[114,115] Here, a Zn^{2+} cation is used to replace $Co^{2+/3+}$ (see Section S6, Scheme S3) to optimize geometries of the differently charged Zn-containing species (as Zn^{2+} can be assumed as redox inert, the metrical charge of the ligand is well-established). Careful analysis (see Section S6 for details) revealed that the metrical charge of the ligand is −1 (see Section S6, Table S7) for all three species **1**−**3**. Thus, one can assign the oxidation state of the central Co atom in these complexes to +2, + 3, and +3, respectively. The obtained charges are further validated by means of localized orbitals that indicate d^7, d^6, and d^6 electronic configuration of Co in the studied complexes **1**−**3** (see Section S6, Table S8), respectively.

The preferred spin state of the ^{2}[**1**]$^+$ complex is a doublet, with the spin density (as well as β-LUMO) being localized at the central Co atom (a mix of $3d_{xz}$ + $3d_{yz}$ AOs); see Figure 6. The formal 3d configuration of Co in ^{2}[**1**]$^+$ is $d_{z^2}^2$ d_{xy}^2 $d_{xz}^{1.5}$ $d_{yz}^{1.5}$ $d_{x^2-y^2}^{0}$ according to d(Co)-like Mulliken population analysis (MPA). BS singlet spin state in ^{u1}[**2**]$^+$ is found just 0.3 kJ/mol below the closed shell ^{1}[**2**]$^+$ (see Section S6, Table S8).

The ^{u1}[**2**]$^+$ spin state has a low S^2 value (0.137) and a low spin density at Co 0.260, of d_{z^2} (Co) AO character, and an

https://doi.org/10.1021/jacsau.4c00005
JACS Au 2024, 4, 1166−1183

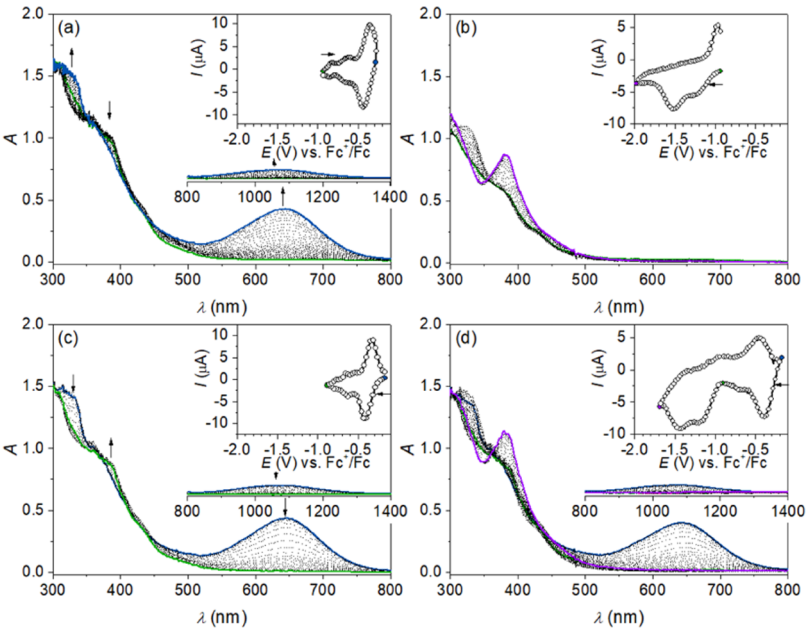

Figure 5. UV−vis−NIR spectra obtained upon the spectroelectrochemical measurement in 0.1 M nBu$_4$NPF$_6$/MeCN: (a) oxidation of **1** and (b) reduction of **1**, as well as (c) first reduction of **2** and (d) first and second reductions of **2**. NIR regions are shown for relevant species. Insets show the corresponding CVs measured with the Pt working electrode at a scan rate of 3 mV s^{-1}. Circles mark potentials where the spectra were sampled, and for highlighted records, the color matches the spectrum line color.

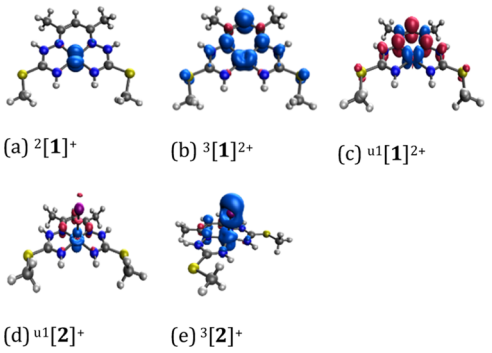

Figure 6. Spin density of chosen species studied, namely, (a) ^{2}[**1**]$^+$, (b) ^{3}[**1**]$^{2+}$, (c) ^{u1}[**1**]$^{2+}$, (d) ^{u1}[**2**]$^+$, and (e) ^{3}[**2**]$^+$; the isosurface value is 0.004 e·bohr^{-3}.

opposite spin density of −0.260 on the ligand (possibly to be considered as a half-electron BS open shell system, see Figure 6d and Table S8). Nevertheless, according to the localized orbitals, in both ^{u1}[**2**]$^+$ and ^{1}[**2**]$^+$, the central Co atom is in the oxidation state +3 (d^6 electronic configuration for all considered spin states is found, see Table S8). The formal 3d configuration of ^{1}[**2**]$^+$ is d_{xy}^2 d_{xz}^2 d_{yz}^2 according to d(Co)-like MPA. In the case of ^{1}[**3**]^0, the restricted singlet state is found preferred (see Table S8) with a d^6 electronic configuration of cobalt (d_{xy}^2 d_{xz}^2 d_{yz}^2 electronic configuration). In the case of dimer [**4**]^0, the restricted singlet spin state is preferred (see Section S6, Table S8) with a d^6 electronic configuration on both cobalt atoms (d_{xy}^2 d_{xz}^2 d_{yz}^2 electronic configuration), like in ^{1}[**3**]^0. All of the findings are in accordance with the XAS results and sharpen the experimental results of the studied species **1**−**3**.

Considering the electrochemistry of **1** and **2**, the frontier orbitals are worth to be discussed in further detail. The reduction (oxidation) locus of **1** can be directly related to the shapes of the LUMO (HOMO) orbitals. The LUMO has a 61% $d_{x^2-y^2}$ Co character (see Section S5, Figure S20e), suggesting the reduction of Co^{II} to Co^{I} (physical charge +2 to +1) in **1**, despite the coordination of the axial coligand being deterministic for the redox locus assessment (vide supra). The analysis of localized orbitals and (MPA d-populations) suggests that the central atom is the reduction locus, but due to the ligand−metal noninnocent character, the situation is not a pure resonance structure with Co^{I} (one localized Co 3d orbital of **1** after reduction is occupied only by 1.7 electrons, and the MPA AO d-populations are shifted from the ideal value of two). Thus, the reduction of **1** can also partially affect the ligand (to ca. 25%). Notably, the oxidation locus of **1** is the ligand, when the axial position is left out of coordination, according to the β-HOMO (see Figure S20g), which is energetically above the α-HOMO Figure S20d. On the other hand, XAS and theoretical approaches identify Co^{III} in **2**. The α- and β-HOMO of **2** have 10 and 9% Co d_{z^2} character (for the α- and β-LUMO, the corresponding values are 30 and 52%). Hence, the oxidation (locus relevant to HOMO) does not involve the central atom to a large extent in **1**, while especially the high Co d_{z^2} character of β-LUMO (notice the singlet unrestricted BS regime) points to the Co atom as the reduction locus of **2**, i.e., Co^{III} is reduced to Co^{II}. According to these findings, one has to hypothesize that the coordination of **1** and **2** is essentially the same in MeCN solution, i.e., iodide—which is contained in both **1**, as the counteranion, and **2**, within the coordination sphere—is either replaced by MeCN (upon dissolving or reduction) or plays a dynamic role in the redox cycle, leading to the same cyclic voltammograms for the first oxidation of **1** and reduction of **2** of the Co^{II}/Co^{III} couple.

Catalytic Studies

While investigating the potential for the catalysis of cobalt(III) complexes **2** and **3**,[69,77,116−118] we found that in the presence of $PhSiH_3$ and dioxygen,[119] 2-vinylnaphthalene (**9a**) could be oxidized to the corresponding ketone (**10a**) in a Wacker oxidation-type fashion (cf. Scheme 2). Particularly striking is

https://doi.org/10.1021/jacsau.4c00005
JACS Au 2024, 4, 1166−1183

Table 1. Optimization of the Reaction Conditions[a]

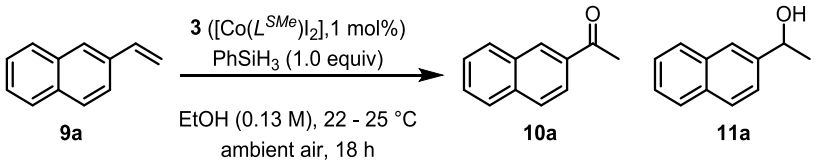

entry	deviation from standard conditions	yield of **10a** (%)
1	none	80 (76)
2	**2** ([Co(H$_2$L^{SMe})I]I) instead of **3** ([Co(L^{SMe})I$_2$])	72[b]
3	**4** ([Co^{III}(L^{SMe,O})I]$_2$) instead of **3**	26
4	PMHS instead of PhSiH$_3$	29
5	0.5 M instead of 0.13 M	67
6	O$_2$ atmosphere instead of ambient air	74
7	No precatalyst	<5
8	No PhSiH$_3$	<5
9	anoxic solvent + Ar atmosphere instead of ambient air	<5

[a]Reactions were performed on a 0.5 mmol scale and yields were quantified by ^{1}H NMR using 1,3,5-trimethoxybenzene as the internal standard. The isolated yield is given in parentheses. [b]An increase in the amount of undesired alcohol (**11a**) was also observed.

Chart 1. Scope of Oxidized Products[a]

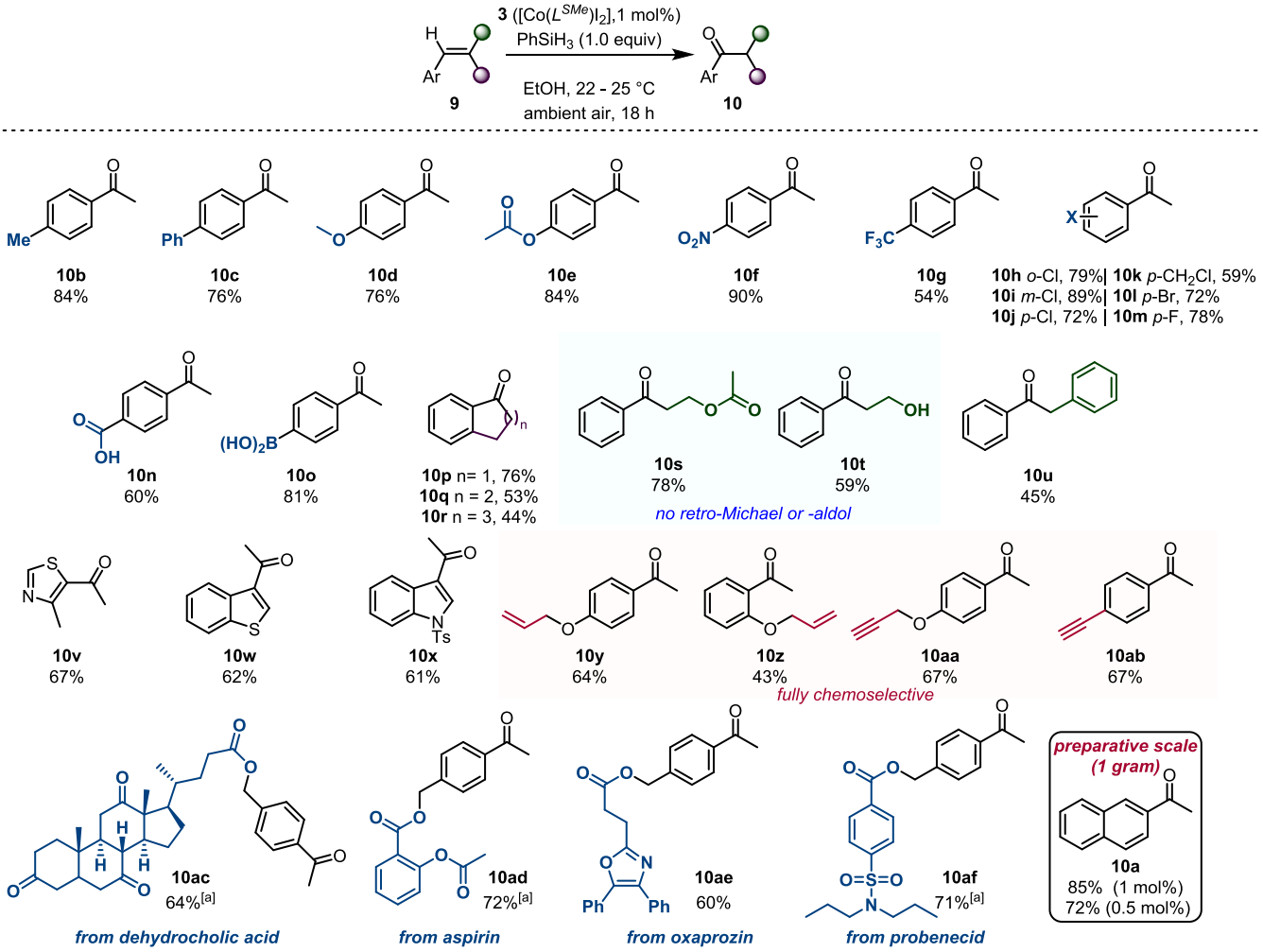

[a]Reactions were performed on a 0.5 mmol scale. All yields refer to isolated materials. Tetrahydrofuran (THF) was used instead of EtOH due to solubility issues.

the fact that, while the conditions are reminiscent of the Mukaiyama hydration of alkenes to alcohols (cf. Scheme 4a), the process we uncovered almost exclusively delivers ketones as the reaction products (cf. Scheme 4b). While this selectivity is not entirely unknown, as evidenced by a seminal report by Matsushita,[71] the underlying strategy did not retain the

https://doi.org/10.1021/jacsau.4c00005
JACS Au 2024, 4, 1166−1183

attention of the community—at least in part, as it suffered from the inconvenient requirement for an O_2 atmosphere.

Following the discovery of the ability of complex **3** to oxidize **9a** to **10a**, we embarked on optimization of the reaction. Remarkably, using a catalyst loading of only 1 mol %, in the presence of $PhSiH_3$ in EtOH at room temperature and under exposure to ambient air, a high yield for the ketone product was obtained (Table 1, entry 1). Complex **2** was also found to be capable of mediating the reaction, but the transformation was found to be less robust (entry 2). Reaction with complex **4** did not lead to any appreciable amounts of product, indicating the necessity for a ligand capable of participating in redox events (entry 3).[120] Substitution of $PhSiH_3$ for the silicon industry byproduct polymethylhydrosiloxane (PMHS) resulted in a drastic decrease in yield (entry 4), while the negative effect of performing the reaction under more concentrated conditions was less pronounced (entry 5), and the use of a pure O_2 atmosphere proved to have little effect (entry 6). Control experiments conducted in the absence of complex **3**, without $PhSiH_3$ or under anoxic conditions did not yield any product (entries 7−9). To demonstrate that alcohol **11a** was not formed by the reduction of the ketone with $PhSiH_3$, acetophenone was exposed to the reaction conditions but remained intact.

Having established optimized reaction conditions, the applicability of the transformation to different olefins was investigated (Chart 1). A wide range of substituents on the phenyl ring, including various functional groups with different electronic effects, were successfully oxidized in a fully regioselective manner (**10b−o**). As illustrated by the series of chloro-substituted derivatives, the reaction was not limited to *para* substituents but also tolerated *ortho* and *meta* substitution (**10h−j**). 1,2-Disubstituted styrenes, either in their cyclic or linear form, afforded the desired products in moderate to good yields (**10p−u**), and the mild reaction conditions allowed for the preparation of products **10s** and **10t** without the formation of retro-Michael or retro-Aldol byproducts. Given the importance of heterocycles in the discovery of new biologically active compounds, we investigated the tolerance of this protocol toward a range of electron-rich heterocycle-substituted alkenes, with the obtention of **10v−x** underlining the chemoselectivity of this oxidation. In addition, the chemoselectivity of the transformation using substrates containing other alkene- or alkyne substituents was studied. We were pleased to find that the reaction displayed complete selectivity for styrene-like olefins, leaving all other unsaturation untouched (**10y−ab**). Moreover, the applicability of the transformation to more complex substrates derived from natural products or pharmaceuticals was also investigated. Gratifyingly, we found that, even in these more complex scenarios, the reaction proved to be robust, and the products could be obtained in good yields (**10ac−af**). Finally, to demonstrate the scalability of oxidation, 1 g of model substrate **9a** was subjected to the reaction conditions, providing **10a** in high yield—in this context, we also showed that the catalyst loading could be reduced to 0.5 mol % without significant deterioration of the isolated yield.

Apart from the potential synthetic utility of the method, the mechanistic aspects and its deviation from the venerable Mukaiyama reaction are intriguing. Therefore, we performed a series of experiments to gain insight into the mechanism of this catalytic reaction.

Insight into the Mechanism of Catalytic Oxidation

Initially, poisoning experiments were conducted in order to assess whether catalysis occurs under homogeneous or heterogeneous conditions. Thus, while the presence of PPh_3 or pyridine led to diminished yields being obtained, addition of elemental Hg did not lead to a significant change (see Section S7 for details). These results support the notion of homogeneous catalysis and the noninvolvement of Co nanoparticles. The fact that, under inert atmosphere and in an anoxic solvent, no desired product could be observed (Table 1, entry 9) suggests that air dioxygen is most likely incorporated into the products. Next, to rule out an autoxidation mechanism, we conducted the reaction in the presence of butylated hydroxytoluene (BHT), an efficient oxygen-centered radical trap (Scheme 6a).[121] Notably, **10a** was

Scheme 6. Additional Mechanistic Studies[a]

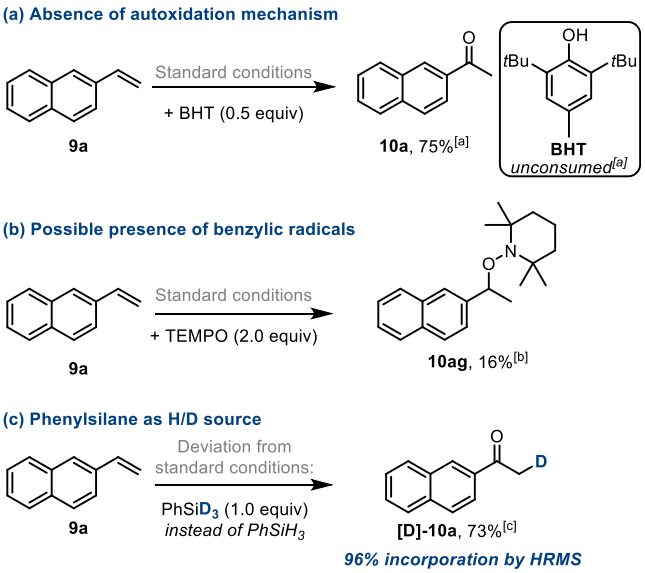

[a](a) The addition of BHT (dibutylhydroxytoluene) indicates a mechanism other than autoxidation. (b) Observation of TEMPO-adduct **10ag** points toward the involvement of a benzylic radical. (c) Crucial role of the reducing agent (phenylsilane) in promoting the reaction. [a] NMR yield. [b] NMR conversion. [c] Isolated yield.

formed in the expected yield, while BHT remained unconsumed. In addition, replacing the catalyst with an organic initiator such as azobis(isobutyronitrile) (AIBN) did not result in any conversion.[121] These collected data suggest that highly reactive oxygen species are not involved in the oxidation process. Other mechanistic possibilities such as alkene hydration and subsequent dehydrogenation or Meinwald rearrangement[122] were also excluded due to the lack of reactivity of 1-(2-naphthyl)ethanol or styrene oxide under standard conditions. Subsequently, when 2,2,6,6-tetramethyl-1-piperidinyloxy (TEMPO) was used as an additive, most of the reactivity was quenched, but we were able to identify the TEMPO-adduct **10ag**, suggesting the formation of a benzylic radical (Scheme 6b).

As a control, in the absence of complex **3**, no detectable amount of **10ag** was found. Finally, when deuterated phenylsilane ($PhSiD_3$) was used as the reducing agent, 96% deuterium incorporation in the methyl group was obtained, as measured by HRMS (see Scheme 6c and Section S7 for

https://doi.org/10.1021/jacsau.4c00005
JACS Au 2024, 4, 1166−1183

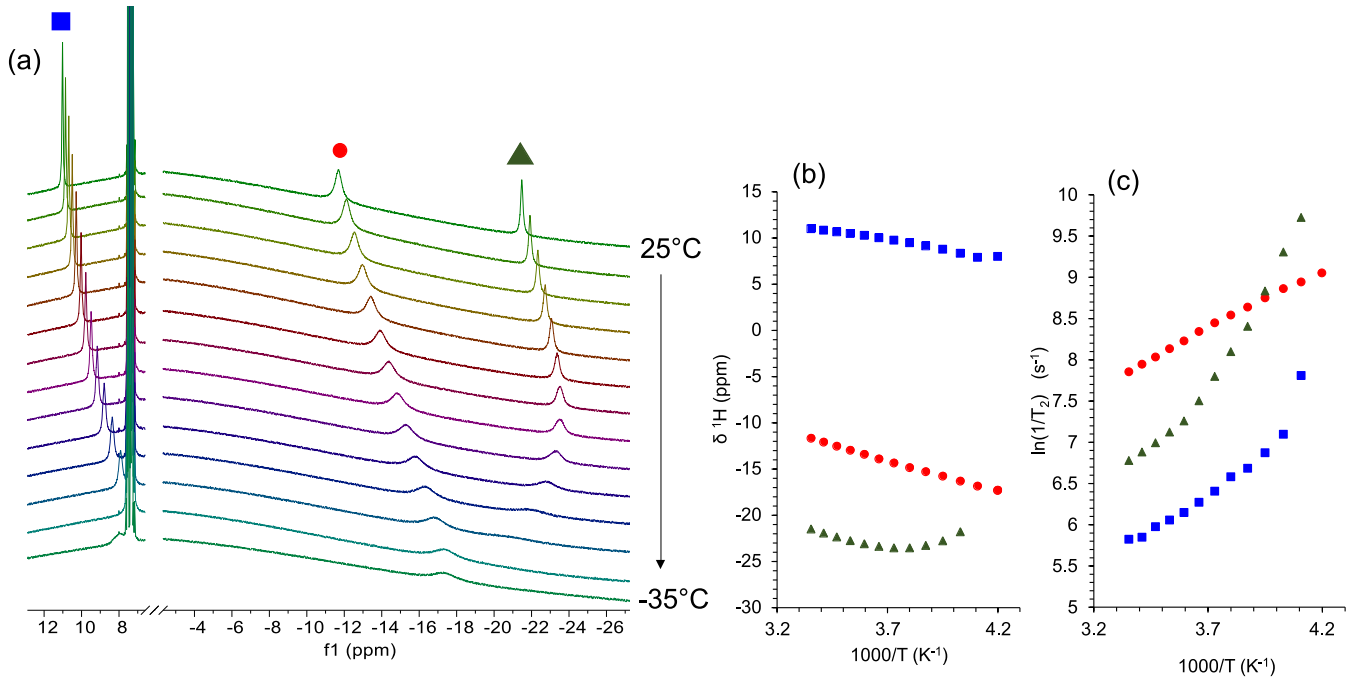

Figure 7. (a) Stack plots of ^{1}H NMR spectra for **2** + $PhSiH_3$ in MeOH-d_4 in the temperature range from 25 to −35 °C; (b) temperature dependence of the chemical shifts for paramagnetic signals displayed in panel (a); and (c) evolution of transverse relaxation rates $1/T_2$ of the three resonance signals in panel (a).

details), while the use of $PhSiH_3$ in EtOD did not lead to any labeling. Typically, the mechanism of the Mukaiyama hydration is represented by the formation of Co−H species after reduction by a silane.[118] However, considering the studies of Peters[123] and Norton,[124] in which the formation of transient Co(III)−H species within the cobaloxime system was questioned, we decided to study the reduction of the precatalysts used (**2** and **3**) by $PhSiH_3$ in more detail.

The chemical transformations of $PhSiH_3$ in MeOH-d_4 in the presence of complex **2** (0.3:1) and in its absence were investigated by ^{1}H and ^{29}Si NMR spectroscopy.[125]

In the absence of **2**, the spectra remain practically time-independent, while the presence of **2** elicits significant changes, leading to almost complete disappearance of the quartet signal between 7.32 and 7.37 ppm after 155 min, implying solvolysis of $PhSiH_3$ (see Section S7, Figure S80). Similarly, ^{29}Si NMR spectra were measured over time (60 min), again in the presence and absence of **2** (see Section S7, Figure S81). We noticed that the ^{29}Si resonance of $PhSiH_3$ at $\delta(^{29}Si)$ = −61.16 ppm decreased gradually in the presence of **2** and three additional signals appeared at −14.90, − 26.23, and −54.56 ppm. While the former two resonances disappeared over time, the third signal reached maximal intensity after the first two species had disappeared completely. These time-dependent spectra mirror the consecutive dehydrogenative coupling of $PhSiH_3$ with MeOH-d_4 mentioned in many other catalytic studies.[62,65,66,126−129] Stepwise formation of $PhSiH_2(OCD_3)$, $PhSiH(OCD_3)_2$, and $PhSi(OCD_3)_3$ in the presence of **2** was confirmed by the measurement of the ^{29}Si signal of $PhSi(OCH_3)_3$ and compared with the time-independent spectra of $PhSiH_3$ measured in the absence of **2** (see Figure S81). It is worth noting that Ph(*i*-Pr−O)SiH_2 has been found to be an exceptionally efficient reductant in catalytic reactions,[130] with detailed mechanistic pictures of such transformations recently reported.[131]

The ^{1}H NMR spectrum of the SCD_3-labeled complex **2** in the presence of $PhSiH_3$ (1 equiv) in MeOD-d_4 after 24 h showed a singlet at 4.46 ppm and a 1:1:1 triplet at 4.42 ppm with $J_{HD} \approx 43$ Hz (Figure S82), which can be attributed to H_2 and HD, respectively, in solution.[132,133]

Interestingly, in a ^{1}H NMR spectrum recorded at room temperature, the signals of the initial complex **2** disappeared and four new signals, at 11.02 and −11.67 ppm (attributed to one species) and 4.20 and −21.48 ppm (attributed to a second distinct species), emerged. The line width of the four proton resonances is large and the chemical shifts are spread into the negative region of the spectrum, which is not typical for diamagnetic species and therefore potentially point to the existence of two paramagnetic Co(II) species.[123] However, similar signals in the negative range have also been attributed to Co(III)−H[124,132] or to transient Co(I)−H species[129] in hydrogenation reactions.

To get more insight into the nature of cobalt species formed by the reaction of **2** with $PhSiH_3$, we measured ^{1}H NMR spectra in MeOH-d_4 in the temperature window from 25 to −35 °C and investigated the temperature dependence of the chemical shifts and the relaxation times of three out of the four prominent resonances. The fourth signal, at 4.20 ppm, was not involved in this analysis, as it partially overlapped with other resonances. A strong temperature dependence of the chemical shifts and a significant resonance line broadening upon temperature decrease[134,135] (Figure 7) indicated the presence of the paramagnetic Co(II) species.[136−140]

Given the reducing properties of phenylsilane, the formation of Co(II) complex **1** was considered likely. The comparison of the ^{1}H NMR spectrum of **1** in MeOH-d_4 with the NMR spectrum of the reaction system **2** + $PhSiH_3$ at the same temperature showed the coincidence of the two broad resonances of **1** with the two of the four resonances observed for the reaction mixture **2** + $PhSiH_3$ (Figure S83). In addition,

https://doi.org/10.1021/jacsau.4c00005
JACS Au 2024, 4, 1166−1183

Scheme 7. Possible PCET in the Oxidation Processes of the Reduced Phenylsilane Complex; * Only One of Three Resonance Forms of $(L^{SMe\bullet\bullet})^{2-}$ is Shown; All Three Resonance Structures Are Displayed in Chart S1 (see Section S8)

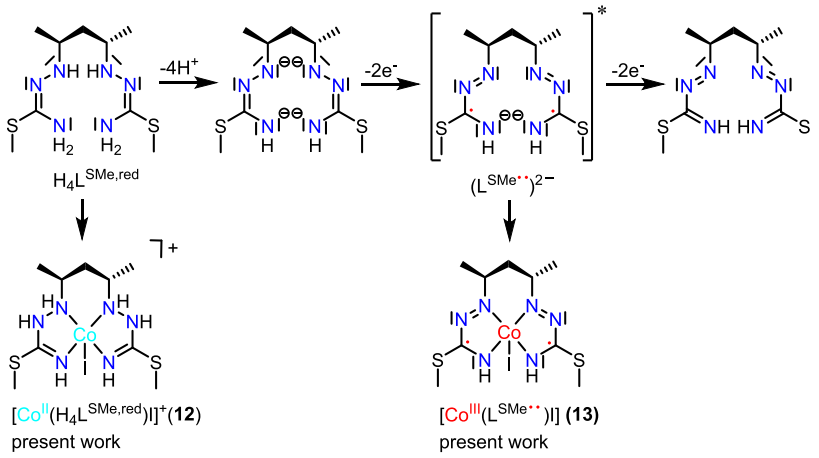

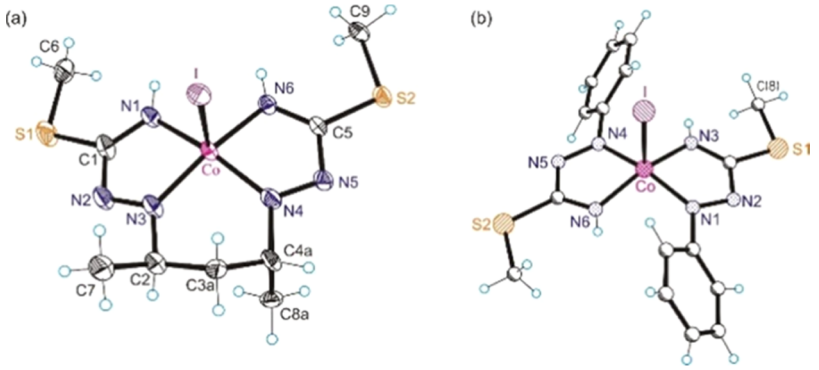

Figure 8. (a) ORTEP view of the Co(III) complex $[Co^{III}(L^{SMe\bullet\bullet})I]$ (**13**) with a trianionic ligand diradical with the atom labeling scheme and thermal ellipsoids drawn at 50% probability level; and (b) ball-and-stick view of the Co(III) complex $[Co^{III}(Q^{Me\bullet})_2I]$.[141,142]

SCD_3 labeling allowed for the identification of the SCH_3 resonances. Furthermore, integration of the resonances permitted the assignment of another signal to methyl groups of the Hacac moiety. These findings indicate that complex **1** is one of the products of the reaction of **2** with $PhSiH_3$, while the other two resonances present in the ^1H NMR spectrum likely arise from another paramagnetic Co(II) species formed. Attempts to identify this second species were successful as well.

Further Investigation of Potentially Catalytically Active Cobalt Complexes and Ligand Noninnocence

The reaction of **2** with $PhSiH_3$ (1 equiv) in MeCN in a closed NMR tube after long standing at room temperature generated green crystals of X-ray diffraction quality, which were studied by SC-XRD and confirmed the formation of complex **12** (Scheme 7 and Section S8, Figure S84). The reduced reaction mixture of **2** with $PhSiH_3$ (1 equiv) in a closed NMR tube in MeOH-d_4 was allowed to stand at room temperature with very slow diffusion of air into the closed tube with the formation of a violet-red solution at the top of the tube (see Section S8, Figure S85) from which single crystals of X-ray diffraction quality of **13** were isolated and investigated by SC-XRD. The result is shown in Figure 8a.

The comparison of the metrical parameters in **13** ($[Co^{III}(L^{SMe\bullet\bullet})I]$, Figure 8a) with those in a previously described square-pyramidal Co(III) complex with two 1-phenylisothiosemicarbazide monoanionic ligand radicals *trans*-$[Co^{III}(Q^{Me\bullet})_2I]$ (Figure 8b) led to the conclusion that a diradical species must be present.[142] This implies that the investigated crystals have been obtained by air oxidation of **12**, forming a dianionic diradical Co(III) species **13**. The collected evidence suggests that this last species resulted from $2e^-$ oxidation of Co(II) complex **12** and release of four protons from the ligand (Scheme 7).

As the precise localization of the unpaired electrons of the diradical species **13** was not clear, further comparison with literature precedent[138] was performed. *S*-Methyl-1-phenyl-isothiosemicarbazide (H_2Q^{Me}), in the presence of air oxygen, was recently shown to bind in a *N*,*N*-mode to cobalt(III) (as well as nickel(II) and iron(III)) in the $1e^-$ oxidized form as the monoanionic ligand radical $(Q^{Me\bullet})^{1-}$.[141−143]

Comparison of the two C−N and N−N bond distances in the ligand in complex $[Co^{III}(Q^{Me\bullet})_2I]$[139,140] (Figure 8b) and in **13** (Figure 8a) revealed close similarity of the corresponding metrical parameters, as shown in Chart 2. Based on this, we can assign the oxidation level of the ligand as π-diradical dianion $(L^{SMe\bullet\bullet})^{2-}$.[144]

To further corroborate our findings, DFT calculations of **13** were performed. For this, we considered two possible scenarios: (i) both unpaired electrons of the diradical species could be situated on the ligand (as indicated in **13**—$[Co^{III}(L^{SMe\bullet\bullet})I]$) or (ii) an electron each could be localized on the ligand and on cobalt ($[Co^{\bullet}(L^{SMe\bullet})I]$). Broken-symmetry singlets (u1) with antiparallel spins on the central Co ion and the ligand in $[Co^{\bullet}(L^{SMe\bullet})I]$, resulted from DFT calculations, providing further evidence for a diamagnetic

https://doi.org/10.1021/jacsau.4c00005
JACS Au 2024, 4, 1166−1183

Chart 2. Metric Parameters of the Five-Membered Chelate Ring(s) in *trans*-$[Co^{III}(Q^{Me\bullet})_2I]$ from Refs 141,142 and in $[Co^{III}(L^{SMe\bullet\bullet})I]$ (13) Reported Herein; Only One Resonance Structure is Shown for Both Complexes[a]

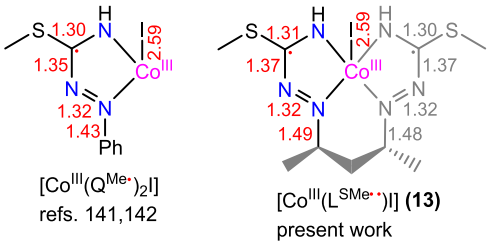

$[Co^{III}(Q^{Me\bullet})_2I]$
refs. 141,142

$[Co^{III}(L^{SMe\bullet\bullet})I]$ **(13)**
present work

[a]Adapted partly from ref 142, American Chemical Society, Copyright (2004).

ground state $S = 0$ (see Figure 9 and Section S8, Table S11), as was also the case for *trans*-$[Co^{III}(Q^{Me\bullet})_2I]$, which gives a ^1H

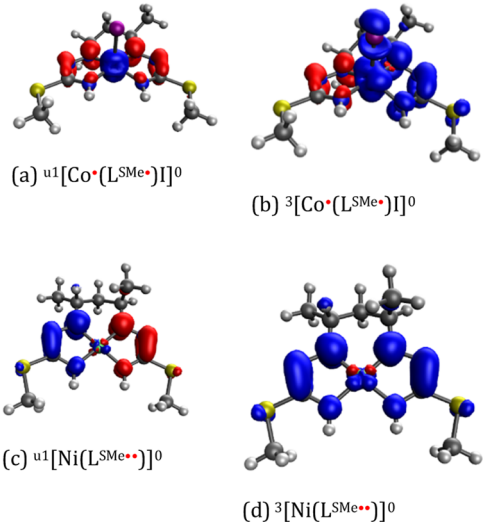

(a) $^{u1}[Co^{\bullet}(L^{SMe\bullet})I]^0$

(b) $^3[Co^{\bullet}(L^{SMe\bullet})I]^0$

(c) $^{u1}[Ni(L^{SMe\bullet\bullet})]^0$

(d) $^3[Ni(L^{SMe\bullet\bullet})]^0$

Figure 9. Spin density of chosen species $[Co^{\bullet}(L^{SMe\bullet})I]$ and $[Ni(L^{SMe\bullet\bullet})]$ studied; the isosurface value is 0.004 e·bohr^{-3}.

NMR spectrum typical for diamagnetic compounds (see Section S8, Figure S86). Here, we have to emphasize that the Co oxidation state is rather unresolved and/or an intermediate oxidation state. One reasonable resonance structure (bonding picture) to mention is likely a Co^{II} with a strong π back-donation to the ligand that results in the unresolved oxidation state. This has been further confirmed in the absence of iodido ligand (see Section S8, Table S11). In contrast, by calculation, we observed a ligand−biradical interaction in the case of other diamagnetic complexes $[Ni(L^{SMe\bullet\bullet})]$ (Figure 9 and Table S11) and $[Zn(L^{SMe\bullet\bullet})]$ (Table S11), where the existence of antiferromagnetic $S = 0$ states was previously reported for a similar square-planar complex $[Ni^{II}(Q^{Me\bullet})_2]$.[86]

Other Mechanistic Considerations

Complex **3** was shown to be reduced to **1** by 1 equiv of $PhSiH_3$ in methanol and reoxidized by slow air oxygen supply back to **3**, as confirmed by SC-XRD.

Formation of dimeric di-Co(III) complex $[Co^{III}(L^{SMe,O})I]_2$ (**4**) and its monomeric counterpart $[Co^{III}(L^{SMe,O})I(CH_3OH)]$ (**5**) (see Section S2 and Scheme S2) is assumed to occur via activation of molecular oxygen by square-planar or square-pyramidal Co(II) complexes with the formation of intermediate Co(III) peroxido species (**D**, Scheme 8).[145] This is

Scheme 8. Proposed Intermediate D Presumably Involved in Catalysis

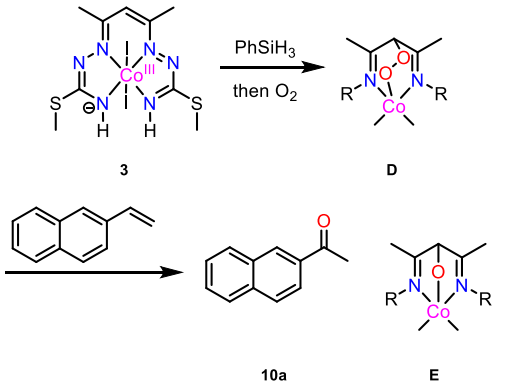

supported by reported $^{18}O_2$ labeling experiments with redox-active copper(II) complexes, which revealed that the oxygen atom in the ketone diimine product originated from molecular oxygen.[146] Additionally, activation of O_2 by five-coordinate Pt(IV) complexes was recently disclosed to occur with the involvement of both the electrophilic metal center and a Lewis basic site on the central carbon atom of Hacac, as concluded from the X-ray diffraction structure of a peroxido complex.[147] These Pt(IV) peroxido complexes were shown to be effective oxidants of organic substrates, e.g., PPh_3, Me_2S, or CO. Addition of molecular oxygen to both a cobalt center and a ligand radical with the formation of a Co(III)-peroxido species was also confirmed quite recently by X-ray diffraction.[148,149]

Two identified species from the reaction mixture of **2** with 1 equiv of $PhSiH_3$ appear to be of primary importance for the investigated catalytic transformations. The first, the cobalt(II) complex generated by the reduction of **2** or **3** with $PhSiH_3$, namely, **1**, was found to catalyze the formation of nascent hydrogen. The dehydrogenative reaction of $PhSiH_3$ with MeOH/MeOH-d_4 was found to be minor in the absence of complex **2**, as confirmed by both ^1H and ^{29}Si NMR spectral measurements, as discussed previously. The produced nascent hydrogen is likely involved in the reduction of two azomethine bonds in **1** with the formation of a second paramagnetic Co(II) species, shown as $[Co^{II}(H_4L^{SMe,red})I]I$ (**12**) in Scheme 7, Figure S84, and Scheme S2. This latter complex can be considered as a reservoir of H equivalents stored in the form of C−H/N−H bonds and as a source of H incorporated into the olefin oxidation products. Exposure of both of these species to oxygen afforded complexes with a ligand oxidized at the central carbon atom of the Hacac moiety, i.e., $[Co^{III}(L^{SMe,O})I(CH_3OH)]$ (**5**), or generation of complex $[Co^{III}(L^{SMe\bullet\bullet})I]$ (**13**). The formation of **5** might occur via a transient Co^{III}-peroxido complex (**D**, Scheme 7) in which the O_2^{2-} group bridges the central carbon atom of the Hacac moiety with Co^{III}. **D** could be involved in intramolecular oxidation of the ligand or in intermolecular oxygen-atom transfer, as reported for other Pt(IV) complexes (vide supra). The role of the second species, **13** $[Co^{III}(L^{SMe\bullet\bullet})I]$, in the catalytic transformations is still to be elucidated. However, identification of this species as a cobalt(III) complex with a π-diradical dianionic ligand with a spin ground state $S = 0$ has disclosed a new facet of redox chemistry for the PBIT platform,

https://doi.org/10.1021/jacsau.4c00005
JACS Au 2024, 4, 1166−1183

unprecedented reduction of the two azomethine bonds, and redox noninnocent behavior of the reduced ligand $H_4L^{SMe,red}$ upon oxidation.

CONCLUSIONS

Access to cobalt complexes with the chemically and redox noninnocent PBIT ligand and their comprehensive characterization are reported. The factors that make the PBIT system particularly attractive as a platform for disclosure of unexplored chemistry include the capacity to stabilize Co and the ligand in two different physical oxidation states at relatively modest potentials, along with an impressive flexibility in coordination numbers and geometry, as well as the adopted protonation states and reactivity of the ligands. Several discernible protonation states of the ligand have been elucidated by spectroscopic and SC-XRD analyses of cobalt(II) and cobalt(III) complexes. The ligand in $[Co^{III}(L^{SMe})I_2]$ proved to be a 12π electronic monoanionic system resulting from $2e^-$ oxidation of the 14π trianionic ligand $(L^{SMe})^{3-}$. The oxidation states +3 for Co and −1 for the tetradentate ligand in the six-coordinate di-iodido complex $[Co^{III}(L^{SMe})I_2]$ were corroborated by X-ray absorption spectra and inspection of metrical parameters in the PBIT ligand resulting from SC-XRD studies. Slow oxidation of complex $[Co^{II}(H_4L^{SMe,red})I]I$ (**12**) obtained by reduction of $[Co^{III}(H_2L^{SMe})I]I{\cdot}CH_3OH$ with 1 equiv of $PhSiH_3$ in methanol afforded an unprecedented cobalt(III) complex with a dianionic diradical ligand formulated as $[Co^{III}(L^{SMe\bullet\bullet})I]$ (**13**). The ligand in **12** was found to remotely incorporate four equivalents of hydrogen when compared to the coordinated ligand H_3L^{SMe} (Scheme S1), which are stored in the form of C−H or N−H bonds, a thus far unexplored feature of the PBIT platform. Effective hydrogen storage implies reversible addition and release of H atoms,[150] which still has to be confirmed. Multiproton-responsive ligands[151] have already been successfully used in important chemical transformations and are expected to be valorized in the future. The described complexes, in combination with $PhSiH_3$ as the reductant, ambient air as the oxidant, and ethanol as the solvent, offer a simple catalytic system for the chemo- and regioselective oxidation of styrene-like olefins to their corresponding ketones. The transformations proceed at room temperature and with good efficiency, with a low precatalyst loading (down to 0.5 mol %). In addition to a broad functional group tolerance, the established protocol proved to be suitable for late-stage oxidation of molecules derived from natural products. As catalytically competent species, the cobalt(II) complex with a fully reduced ligand, $[Co^{II}(H_4L^{SMe,red})I]I$, and cobalt(III)−peroxido complex have been suggested based on insights into the mechanism of the catalytic oxidation of olefins. Attempts to spectroscopically identify and characterize the cobalt(III)-peroxido complex by SC-XRD are ongoing in our laboratory.

METHODS

General Procedure for the Cobalt-Catalyzed Wacker-Type Oxidation

The olefin substrate (0.5 mmol, 1.0 equiv; either neat, followed by EtOH (4 mL) or as a solution in EtOH (4 mL)) was added to a vial containing the Co precatalyst **3** (2.9 mg, 1 mol %) and a stirring bar. The mixture was then stirred at 1000 rpm, without being in direct contact with the stirring plate. After 1 min, phenylsilane (62 μL, 0.5 mmol, 1.0 equiv) was added and the reaction mixture was stirred for 18 h at room temperature (22−27 °C) under ambient atmosphere. Following full conversion of the olefin, as determined by TLC analysis of the reaction mixture, volatile components were removed under reduced pressure, and the resulting crude material purified by flash chromatography on silica gel using a suitable solvent system.

ASSOCIATED CONTENT

Supporting Information

The Supporting Information is available free of charge at https://pubs.acs.org/doi/10.1021/jacsau.4c00005.

Synthesis, experimental, and computational details; further characterization data of the complexes (CHN combustion analyses, ^{1}H NMR, UV−vis−NIR electron absorption spectra, additional XAS data with associated TDDFT calculations), computational results, single-crystal X-ray crystallographic data, and details of data collection along with the characterization of 32 oxidation products resulting from catalytic oxidation reactions (PDF)

Accession Codes

CCDC 2259330−2259341 contain the supplementary crystallographic data for this paper. These data can be obtained free of charge via www.ccdc.cam.ac.uk/data_request/cif, or by emailing data_request@ccdc.cam.ac.uk, or by contacting The Cambridge Crystallographic Data Centre, 12 Union Road, Cambridge CB2 1EZ, UK; fax: + 44 1223 336033.

AUTHOR INFORMATION

Corresponding Authors

Serena DeBeer − *Max Planck Institute for Chemical Energy Conversion, 45470 Mülheim an der Ruhr, Germany;* orcid.org/0000-0002-5196-3400; Email: serena.debeer@cec.mpg.de

Nuno Maulide − *University of Vienna, Institute of Organic Chemistry, A-1090 Vienna, Austria;* orcid.org/0000-0003-3643-0718; Email: nuno.maulide@univie.ac.at

Vladimir B. Arion − *University of Vienna, Institute of Inorganic Chemistry, A-1090 Vienna, Austria;* orcid.org/0000-0002-1895-6460; Email: vladimir.arion@univie.ac.at

Authors

Vincent Porte − *University of Vienna, Institute of Organic Chemistry, A-1090 Vienna, Austria*

Miljan N. M. Milunovic − *University of Vienna, Institute of Inorganic Chemistry, A-1090 Vienna, Austria*

Ulrich Knof − *Novartis Pharma AG, CH-4056 Basel, Switzerland*

Thomas Leischner − *University of Vienna, Institute of Organic Chemistry, A-1090 Vienna, Austria*

Tobias Danzl − *University of Vienna, Institute of Organic Chemistry, A-1090 Vienna, Austria*

Daniel Kaiser − *University of Vienna, Institute of Organic Chemistry, A-1090 Vienna, Austria;* orcid.org/0000-0001-8895-9969

Tim Gruene − *University of Vienna, Institute of Inorganic Chemistry, A-1090 Vienna, Austria;* orcid.org/0000-0002-8873-4978

Michal Zalibera − *Institute of Physical Chemistry and Chemical Physics, Faculty of Chemical and Food Technology, Slovak University of Technology in Bratislava, SK-81237 Bratislava, Slovak Republic;* orcid.org/0000-0002-6527-1982

Ingrid Jelemenska − *Institute of Physical Chemistry and Chemical Physics, Faculty of Chemical and Food Technology, Slovak University of Technology in Bratislava, SK-81237 Bratislava, Slovak Republic*

Lukas Bucinsky − *Institute of Physical Chemistry and Chemical Physics, Faculty of Chemical and Food Technology, Slovak University of Technology in Bratislava, SK-81237 Bratislava, Slovak Republic;* orcid.org/0000-0002-0190-3231

Sergio A. V. Jannuzzi − *Max Planck Institute for Chemical Energy Conversion, 45470 Mülheim an der Ruhr, Germany;* orcid.org/0000-0001-7406-6633

Ghenadie Novitchi − *CNRS-LNCMI, 38042 Grenoble, France;* orcid.org/0000-0002-6109-6937

Complete contact information is available at: https://pubs.acs.org/10.1021/jacsau.4c00005

Author Contributions

[▽]V.P. and M.N.M.M. contributed equally to this work. CRediT: **Vincent Porte** investigation; **Miljan N. M. Milunovic** investigation, writing-review & editing; **Ulrich Knof** investigation; **Thomas Fabian Leischner** investigation; **Tobias Danzl** investigation; **Daniel Kaiser** writing-review & editing; **Tim Gruene** formal analysis; **Michal Zalibera** investigation; **Ingrid Jelemenska** investigation; **Lukas Bucinsky** investigation; **Sergio A. Venturinelli Jannuzzi** investigation; **Serena DeBeer** writing-review & editing; **Ghenadie Novitchi** investigation; **Nuno Maulide** supervision, writing-review & editing; **Vladimir B. Arion** conceptualization, investigation, supervision.

Notes

The authors declare no competing financial interest.

■ ACKNOWLEDGMENTS

V.B.A. and M.N.M.M. are thankful to Austrian Science Fund (FWF) for financial support of this work through Grant No. I4729. V.P., T.L., T.D., D.K., and N.M. acknowledge the European Research Council (ERC CoG 682002) and the University of Vienna for generous funding. S.A.V.J. and S.D. thank the Max Planck Society for funding. Dr. Laure Decamps and Dr. Casey van Stappen are thanked for helping with the beamline experiment. The authors acknowledge DESY (Hamburg, Germany), a member of the Helmholtz Association HGF, for the provision of experimental facilities. Parts of this research were carried out at PETRA III and the authors thank Dr. Wolfgang Caliebe and Dr. Akhil Tayal for assistance in using P64 beamline. Beamtime was allocated for proposal I-20200656. The authors are also indebted to Dr. Hanspeter Kählig for kinetic measurements by NMR spectroscopy and Dr. Agnieszka Nawara-Hultzsch and Mag. Olivera Cvetkovic for the preparation of samples in glovebox. Dr. Adriano Bauer, Dr. Yury Lebedev, and Justin Alich are thanked for preliminary experiments. The authors also thank Dr. Alexander Schnegg for providing access to the EPR facility of MPI CEC. I.J., L.B., and M.Z. acknowledge Projects APVV-19-0024, APVV-20-0213, APVV DS-FR-19-0035, and VEGA (Contract Nos. 1/0139/20, 1/0175/23, and 1/0392/24).

■ REFERENCES

(1) Jørgensen, C. K. Differences between the four halide ligands, and discussion remarks on trigonal-bipyramidal complexes, on oxidation states, and on diagonal elements of one-electron energy. *Coord. Chem. Rev.* **1966**, *1*, 164−178.

(2) Storr, T.; Verma, P.; Pratt, R. C.; Wasinger, E. C.; Shimazaki, Y.; Stack, T. D. P. Defining the electronic and geometric structure of one-electron oxidized copper−bis-phenoxide complexes. *J. Am. Chem. Soc.* **2008**, *130*, 15448−15459.

(3) Chirik, P. J.; Wieghardt, K. Radical ligands confer nobility on base-metal catalysts. *Science* **2010**, *327*, 794−795.

(4) Chirik, P. J. Preface: Forum on redox-active ligands. *Inorg. Chem.* **2011**, *50*, 9737−9740.

(5) van Leest, N. P.; de Zwart, F. J.; Zhou, M.; de Bruin, B. Controlling radical-type single-electron elementary steps in catalysis with redox-active ligands and substrates. *JACS Au* **2021**, *1*, 1101−1115.

(6) Luca, O. R.; Crabtree, R. H. Redox-active ligands in catalysis. *Chem. Soc. Rev.* **2013**, *42*, 1440−1459.

(7) Kaim, W.; Schwederski, B. Non-innocent ligands in bioinorganic chemistry—An overview. *Coord. Chem. Rev.* **2010**, *254*, 1580−1588.

(8) McNeece, A. J.; Jesse, K. A.; Xie, J.; Filatov, A. S.; Anderson, J. S. Generation and oxidative reactivity of a Ni(II) superoxo complex via ligand-based redox non-innocence. *J. Am. Chem. Soc.* **2020**, *142*, 10824−10832.

(9) Margulieux, G. W.; Bezdek, M. J.; Turner, Z. R.; Chirik, P. J. Ammonia activation, H_2 evolution and nitride formation from a molybdenum complex with a chemically and redox noninnocent ligand. *J. Am. Chem. Soc.* **2017**, *139*, 6110−6113.

(10) Lohmeyer, L.; Kaifer, E.; Himmel, H.-J. Solvent-induced redox isomerism of cobalt complexes with redox-active bisguanidine ligands. *Inorg. Chem.* **2022**, *61*, 8440−8454.

(11) Lohmeyer, L.; Werr, M.; Kaifer, E.; Himmel, H. Interplay and competition between two different types of redox-active ligands in cobalt complexes: how to allocate the electrons? *Chem. - Eur. J.* **2022**, *28*, No. e202201789.

(12) Bart, S. C.; Chłopek, K.; Bill, E.; Bouwkamp, M. W.; Lobkovsky, E.; Neese, F.; Wieghardt, K.; Chirik, P. J. Electronic structure of bis(imino)pyridine iron dichloride, monochloride, and neutral ligand complexes: a combined structural, spectroscopic, and computational study. *J. Am. Chem. Soc.* **2006**, *128*, 13901−13912.

(13) Shimazaki, Y.; Yajima, T.; Tani, F.; Karasawa, S.; Fukui, K.; Naruta, Y.; Yamauchi, O. Syntheses and electronic structures of one-electron-oxidized group 10 metal(II)−(disalicylidene)diamine complexes (Metal = Ni, Pd, Pt). *J. Am. Chem. Soc.* **2007**, *129*, 2559−2568.

(14) Rotthaus, O.; Jarjayes, O.; Thomas, F.; Philouze, C.; Perez Del Valle, C.; Saint-Aman, E.; Pierre, J.-L. Fine tuning of the oxidation locus, and electron transfer, in nickel complexes of pro-radical ligands. *Chem. - Eur. J.* **2006**, *12*, 2293−2302.

(15) Eisenberg, R.; Gray, H. B. Noninnocence in metal complexes: A dithiolene dawn. *Inorg. Chem.* **2011**, *50*, 9741−9751.

(16) Cazacu, M.; Shova, S.; Soroceanu, A.; Machata, P.; Bucinsky, L.; Breza, M.; Rapta, P.; Telser, J.; Krzystek, J.; Arion, V. B. Charge and spin states in Schiff base metal complexes with a disiloxane unit exhibiting a strong noninnocent ligand character: synthesis, structure, spectroelectrochemistry, and theoretical calculations. *Inorg. Chem.* **2015**, *54*, 5691−5706.

(17) Goswami, M.; Lyaskovskyy, V.; Domingos, S. R.; Buma, W. J.; Woutersen, S.; Troeppner, O.; Ivanović-Burmazović, I.; Lu, H.; Cui, X.; Zhang, X. P.; Reijerse, E. J.; DeBeer, S.; van Schooneveld, M. M.; Pfaff, F. F.; Ray, K.; de Bruin, B. Characterization of porphyrin-Co(III)-'nitrene radical' species relevant in catalytic nitrene transfer reactions. *J. Am. Chem. Soc.* **2015**, *137*, 5468−5479.

(18) Chłopek, K.; Bothe, E.; Neese, F.; Weyhermüller, T.; Wieghardt, K. Molecular and electronic structures of tetrahedral complexes of nickel and cobalt containing *N,N′*-disubstituted, bulky *o*-diiminobenzo-semiquinonate(1−) π-radical ligands. *Inorg. Chem.* **2006**, *45*, 6298−6307.

(19) Chaudhuri, P.; Verani, C. N.; Bill, E.; Bothe, E.; Weyhermüller, T.; Wieghardt, K. Electronic structure of bis(*o*-iminobenzosemiquinonato)metal complexes (Cu, Ni, Pd). The art of establishing physical

oxidation states in transition-metal complexes containing radical ligands. *J. Am. Chem. Soc.* **2001**, *123*, 2213−2223.
(20) Jazdzewski, B. A.; Tolman, W. B. Understanding the copper−phenoxyl radical array in galactose oxidase: contributions from synthetic modeling studies. *Coord. Chem. Rev.* **2000**, *200*−*202*, 633−685.
(21) Chaudhuri, P.; Hess, M.; Flörke, U.; Wieghardt, K. From structural models of galactose oxidase to homogeneous catalysis: efficient aerobic oxidation of alcohols. *Angew. Chem., Int. Ed.* **1998**, *37*, 2217−2220.
(22) Bouwkamp, M. W.; Bowman, A. C.; Lobkovsky, E.; Chirik, P. J. Iron-catalyzed [2π + 2π] cycloaddition of α,ω-dienes: the importance of redox-active supporting ligands. *J. Am. Chem. Soc.* **2006**, *128*, 13340−13341.
(23) van der Vlugt, J. I. Radical-Type Reactivity and catalysis by single-electron transfer to or from redox-active ligands. *Chem. - Eur. J.* **2019**, *25*, 2651−2662.
(24) Sikari, R.; Sinha, S.; Chakraborty, G.; Das, S.; Leest, N. P.; Paul, N. D. C−N cross-coupling reactions under mild conditions using singlet di-radical nickel(II)-complexes as catalyst: N-arylation and quinazoline synthesis. *Adv. Synth. Catal.* **2019**, *361*, 4342−4353.
(25) Sikari, R.; Sinha, S.; Das, S.; Saha, A.; Chakraborty, G.; Mondal, R.; Paul, N. D. Achieving nickel catalyzed C−S cross-coupling under mild conditions using metal−ligand cooperativity. *J. Org. Chem.* **2019**, *84*, 4072−4085.
(26) Smith, A. L.; Hardcastle, K. I.; Soper, J. D. Redox-active ligand-mediated oxidative addition and reductive elimination at square planar cobalt(III): multielectron reactions for cross-coupling. *J. Am. Chem. Soc.* **2010**, *132*, 14358−14360.
(27) Jacquet, J.; Blanchard, S.; Derat, E.; Desage-El Murr, M.; Fensterbank, L. Redox-ligand sustains controlled generation of CF_3 radicals by well-defined copper complex. *Chem. Sci.* **2016**, *7*, 2030−2036.
(28) Storr, T.; Mukherjee, R. Preface for the forum on applications of metal complexes with ligand-centered radicals. *Inorg. Chem.* **2018**, *57*, 9577−9579.
(29) Werr, M.; Kaifer, E.; Enders, M.; Asyuda, A.; Zharnikov, M.; Himmel, H. A copper(I) complex with two unpaired electrons, synthesised by oxidation of a copper(II) complex with two redox-active ligands. *Angew. Chem., Int. Ed.* **2021**, *60*, 23451−23462.
(30) Praneeth, V. K. K.; Ringenberg, M. R.; Ward, T. R. Redox-active ligands in catalysis. *Angew. Chem., Int. Ed.* **2012**, *51*, 10228−10234.
(31) Lu, C. C.; DeBeer George, S.; Weyhermüller, T.; Bill, E.; Bothe, E.; Wieghardt, K. An electron-transfer series of high-valent chromium complexes with redox non-innocent, non-heme ligands. *Angew. Chem., Int. Ed.* **2008**, *47*, 6384−6387.
(32) Vaddypally, S.; Tomlinson, W.; O'Sullivan, O. T.; Ding, R.; Van Vliet, M. M.; Wayland, B. B.; Hooper, J. P.; Zdilla, M. J. Activation of C−H, N−H, and O−H bonds via proton-coupled electron transfer to a Mn(III) complex of redox-noninnocent octaazacyclotetradecadiene, a catenated-nitrogen macrocyclic ligand. *J. Am. Chem. Soc.* **2019**, *141*, 5699−5709.
(33) Kärkäs, M. D.; Åkermark, T.; Johnston, E. V.; Karim, S. R.; Laine, T. M.; Lee, B.-L.; Åkermark, T.; Privalov, T.; Åkermark, B. Water oxidation by single-site ruthenium complexes: using ligands as redox and proton transfer mediators. *Angew. Chem., Int. Ed.* **2012**, *51*, 11589−11593.
(34) Kärkäs, M. D.; Liao, R.-Z.; Laine, T. M.; Åkermark, T.; Ghanem, S.; Siegbahn, P. E. M.; Åkermark, B. Molecular ruthenium water oxidation catalysts carrying non-innocent ligands: mechanistic insight through structure−activity relationships and quantum chemical calculations. *Catal. Sci. Technol.* **2016**, *6*, 1306−1319.
(35) Arion, V. B. Coordination chemistry of S-substituted isothiosemicarbazides and isothiosemicarbazones. *Coord. Chem. Rev.* **2019**, *387*, 348−397.
(36) Haddad, A. Z.; Garabato, B. D.; Kozlowski, P. M.; Buchanan, R. M.; Grapperhaus, C. A. Beyond metal-hydrides: non-transition-metal and metal-free ligand-centered electrocatalytic hydrogen evolution and hydrogen oxidation. *J. Am. Chem. Soc.* **2016**, *138*, 7844−7847.
(37) Haddad, A. Z.; Cronin, S. P.; Mashuta, M. S.; Buchanan, R. M.; Grapperhaus, C. A. Metal-assisted ligand-centered electrocatalytic hydrogen evolution upon reduction of a bis(thiosemicarbazonato)-Cu(II) complex. *Inorg. Chem.* **2017**, *56*, 11254−11265.
(38) van der Meer, M.; Rechkemmer, Y.; Peremykin, I.; Hohloch, S.; van Slageren, J.; Sarkar, B. (Electro)catalytic C−C bond formation reaction with a redox-active cobalt complex. *Chem. Commun.* **2014**, *50*, 11104−11106.
(39) Chen, Y.; Ruppel, J. V.; Zhang, X. P. Cobalt-Catalyzed asymmetric cyclopropanation of electron-deficient olefins. *J. Am. Chem. Soc.* **2007**, *129*, 12074−12075.
(40) Jin, L.-M.; Lu, H.; Cui, Y.; Lizardi, C. L.; Arzua, T. N.; Wojtas, L.; Cui, X.; Zhang, X. P. Selective radical amination of aldehydic C(sp^2)−H bonds with fluoroaryl azides via Co(II)-based metalloradical catalysis: synthesis of N-fluoroaryl amides from aldehydes under neutral and nonoxidative conditions. *Chem. Sci.* **2014**, *5*, 2422−2427.
(41) Jin, L.-M.; Xu, X.; Lu, H.; Cui, X.; Wojtas, L.; Zhang, X. P. Effective synthesis of chiral *N*-fluoroaryl aziridines through enantioselective aziridination of alkenes with fluoroaryl azides. *Angew. Chem., Int. Ed.* **2013**, *52*, 5309−5313.
(42) Lyaskovskyy, V.; Suarez, A. I. O.; Lu, H.; Jiang, H.; Zhang, X. P.; de Bruin, B. Mechanism of cobalt(II) porphyrin-catalyzed C−H amination with organic azides: radical nature and H-atom abstraction ability of the key cobalt(III)−nitrene intermediates. *J. Am. Chem. Soc.* **2011**, *133*, 12264−12273.
(43) van Leest, N. P.; Tepaske, M. A.; Oudsen, J.-P. H.; Venderbosch, B.; Rietdijk, N. R.; Siegler, M. A.; Tromp, M.; van der Vlugt, J. I.; de Bruin, B. Ligand redox noninnocence in $[Co^{III}(TAML)]^{0/-}$ complexes affects nitrene formation. *J. Am. Chem. Soc.* **2020**, *142*, 552−563.
(44) van Leest, N. P.; Tepaske, M. A.; Venderbosch, B.; Oudsen, J.-P. H.; Tromp, M.; van der Vlugt, J. I.; de Bruin, B. Electronically asynchronous transition states for C−N bond formation by electrophilic $[Co^{III}(TAML)]$-nitrene radical complexes involving substrate-to-ligand single-electron transfer and a cobalt-centered spin shuttle. *ACS Catal.* **2020**, *10*, 7449−7463.
(45) Su, X.; McCardle, K. M.; Chen, L.; Panetier, J. A.; Jurss, J. W. Robust and selective cobalt catalysts bearing redox-active bipyridyl-*N*-heterocyclic carbene frameworks for electrochemical CO_2 reduction in aqueous solutions. *ACS Catal.* **2019**, *9*, 7398−7408.
(46) Sandl, S.; Maier, T. M.; van Leest, N. P.; Kröncke, S.; Chakraborty, U.; Demeshko, S.; Koszinowski, K.; de Bruin, B.; Meyer, F.; Bodensteiner, M.; Herrmann, C.; Wolf, R.; von Wangelin, J. A. Cobalt-catalyzed hydrogenations via olefin cobaltate and hydride intermediates. *ACS Catal.* **2019**, *9*, 7596−7606.
(47) Bhunia, M.; Sahoo, S. R.; Shaw, B. K.; Vaidya, S.; Pariyar, A.; Vijaykumar, G.; Adhikari, D.; Mandal, S. K. Storing redox equivalent in the phenalenyl backbone towards catalytic multi-electron reduction. *Chem. Sci.* **2019**, *10*, 7433−7441.
(48) Corcos, A. R.; Villanueva, O.; Walroth, R. C.; Sharma, S. K.; Bacsa, J.; Lancaster, K. M.; MacBeth, C. E.; Berry, J. F. Oxygen activation by Co(II) and a redox non-innocent ligand: spectroscopic characterization of a radical−Co(II)−superoxide complex with divergent catalytic reactivity. *J. Am. Chem. Soc.* **2016**, *138*, 1796−1799.
(49) Lee, C. H.; Dogutan, D. K.; Nocera, D. G. Hydrogen generation by hangman metalloporphyrins. *J. Am. Chem. Soc.* **2011**, *133*, 8775−8777.
(50) Arion, V.; Wieghardt, K.; Weyhermueller, T.; Bill, E.; Leovac, V.; Rufinska, A. Synthesis, structure, magnetism, and spectroscopic properties of some mono- and dinuclear nickel complexes containing noninnocent pentane-2,4-dione bis(*S*-alkylisothiosemi-carbazonate)-derived ligands. *Inorg. Chem.* **1997**, *36*, 661−669.
(51) Gerbeleu, N. V.; Simonov, Yu. A.; Arion, V. B.; Leovac, V. M.; Turta, K. I.; Indrichan, K. M.; Gradinaru, D. I.; Zavodnik, V. E.; Malinovskii, T. I. Transition metal complexes with thiosemicarbazide-

https://doi.org/10.1021/jacsau.4c00005
JACS Au 2024, 4, 1166−1183

based ligands. 14. Iron(IV) complexes with 2,4-pentanedione bis(S-alkylisothiosemicarbazone). Crystal and molecular structure of iodo{2,4-pentanedione bis(S-ethylisothiosemicarbazonato)(3-)} iron-(IV). *Inorg. Chem.* **1992**, *31*, 3264−3268.
(52) Knof, U.; Weyhermüller, T.; Wolter, T.; Wieghardt, K.; Bill, E.; Butzlaff, C.; Trautwein, A. X. How "innocent" are pentane-2,4-dione bis(S-alkylisothiosemicarbazonato) ligands in biomimetic Fe^{II} and Fe^{IV} complexes? *Angew. Chem., Int. Ed.* **1993**, *32*, 1635−1638.
(53) Fráter, G.; Bajgrowicz, J. A.; Kraft, P. Fragrance chemistry. *Tetrahedron* **1998**, *54*, 7633−7703.
(54) Ertl, P.; Schuhmann, T. A Systematic cheminformatics analysis of functional groups occurring in natural products. *J. Nat. Prod.* **2019**, *82*, 1258−1263.
(55) Foley, D. J.; Waldmann, H. Ketones as strategic building blocks for the synthesis of natural product-inspired compounds. *Chem. Soc. Rev.* **2022**, *51*, 4094−4120.
(56) Kürti, L.; Czakó, B. *Strategic Applications of Named Reactions in Organic Synthesis: Background and Detailed Mechanisms*; Elsevier Academic Press: Amsterdam, Boston, 2005.
(57) Sheldon, R. A.; Arends, I. W. C. E.; Hanefeld, U. *Green Chemistry and Catalysis*, 1st ed.; Wiley, 2007.
(58) Fernandes, R. A.; Jha, A. K.; Kumar, P. Recent advances in Wacker oxidation: from conventional to modern variants and applications. *Catal. Sci. Technol.* **2020**, *10*, 7448−7470.
(59) Gandeepan, P.; Müller, T.; Zell, D.; Cera, G.; Warratz, S.; Ackermann, L. 3d transition metals for C−H activation. *Chem. Rev.* **2019**, *119*, 2192−2452.
(60) Shekhar, S.; Ahmed, T. S.; Ickes, A. R.; Haibach, M. C. Recent advances in nonprecious metal catalysis. *Org. Process Res. Dev.* **2022**, *26*, 14−42.
(61) Hill, C. L. Controlled green oxidation. *Nature* **1999**, *401*, 436−437.
(62) Liu, B.; Jin, F.; Wang, T.; Yuan, X.; Han, W. Wacker-type oxidation using an iron catalyst and ambient air: application to late-stage oxidation of complex molecules. *Angew. Chem., Int. Ed.* **2017**, *56*, 12712−12717.
(63) Liu, B.; Han, W. Iron-catalyzed Wacker-type oxidation. *Synlett* **2018**, *29*, 383−387.
(64) Liu, B.; Hu, P.; Xu, F.; Cheng, L.; Tan, M.; Han, W. Nickel-catalyzed remote and proximal Wacker-type oxidation. *Commun. Chem.* **2019**, *2*, 5.
(65) Puls, F.; Knölker, H.-J. Conversion of olefins into ketones by an iron-catalyzed Wacker-type oxidation using oxygen as the sole oxidant. *Angew. Chem., Int. Ed.* **2018**, *57*, 1222−1226.
(66) Puls, F.; Linke, P.; Kataeva, O.; Knölker, H. Iron-catalyzed Wacker-type oxidation of olefins at room temperature with 1,3-diketones or neocuproine as Ligands. *Angew. Chem., Int. Ed.* **2021**, *60*, 14083−14090.
(67) Puls, F.; Seewald, F.; Grinenko, V.; Klauß, H.; Knölker, H. Mechanistic studies on the hexadecafluorophthalocyanine−iron-catalyzed Wacker-type oxidation of olefins to ketones. *Chem. - Eur. J.* **2021**, *27*, 16776−16787.
(68) Zhang, G.; Hu, X.; Chiang, C.-W.; Yi, H.; Pei, P.; Singh, A. K.; Lei, A. Anti-Markovnikov oxidation of β-alkyl styrenes with H_2O as the terminal oxidant. *J. Am. Chem. Soc.* **2016**, *138*, 12037−12040.
(69) Abuhafez, N.; Ehlers, A. W.; de Bruin, B.; Gramage-Doria, R. Markovnikov-Selective Cobalt-Catalyzed Wacker-Type Oxidation of Styrenes into Ketones under Ambient Conditions Enabled by Hydrogen Bonding. *Angew. Chem., Int. Ed.* **2023**, *63*, No. e202316825.
(70) Zombeck, A.; Hamilton, D. E.; Drago, R. S. Novel catalytic oxidations of terminal olefins by cobalt(II)-Schiff base complexes. *J. Am. Chem. Soc.* **1982**, *104*, 6782−6784.
(71) Matsushita, Y.-i.; Matsui, T.; Sugamoto, K. Cobalt(II) porphyrin-catalyzed oxidation of olefins to ketones with molecular oxygen and triethylsilane in 2-propanol. *Chem. Lett.* **1992**, *21*, 1381−1384.
(72) Lin, Y. H.; Williams, I. D.; Li, P. Selective oxidation of styrenes under oxygen catalyzed by cobalt chloride. *Appl. Catal., A* **1997**, *150*, 221−229.
(73) Nishinaga, A.; Yamada, T.; Fujisawa, H.; Ishizaki, K.; Ihara, H.; Matsuura, T. Catalysis of cobalt-Schiff base complexes in oxygenation of alkenes: on the mechanism of ketonization. *J. Mol. Catal.* **1988**, *48*, 249−264.
(74) Yasukawa, T.; Kobayashi, S. Oxygenation of styrenes catalyzed by N-doped carbon incarcerated cobalt nanoparticles. *Bull. Chem. Soc. Jpn.* **2019**, *92*, 1980−1985.
(75) Huang, G.; Wang, L.; Luo, H.; Shang, S.; Chen, B.; Gao, S.; An, Y. Isopropanol as a hydrogen source for single atom cobalt-catalyzed Wacker-type oxidation. *Catal. Sci. Technol.* **2020**, *10*, 2769−2773.
(76) Saussine, L.; Brazi, E.; Robine, A.; Mimoun, H.; Fischer, J.; Weiss, R. Cobalt(III) alkylperoxy complexes. Synthesis, X-ray structure, and role in the catalytic decomposition of alkyl hydroperoxides and in the hydroxylation of hydrocarbons. *J. Am. Chem. Soc.* **1985**, *107*, 3534−3540.
(77) Zhao, K.; Shen, Q.; Tao, Y.; Li, J.; Wang, M.; Li, C.; Xu, B. Atomically dispersed N/O-coordinated cobalt catalyst enables aerobic oxygenation of olefins under ambient conditions. *ACS Catal.* **2023**, *13*, 12591−12600.
(78) Adilina, I. B.; Hara, T.; Ichikuni, N.; Shimazu, S. Oxidative cleavage of isoeugenol to vanillin under molecular oxygen catalysed by cobalt porphyrin intercalated into lithium taeniolite clay. *J. Mol. Catal. A: Chem.* **2012**, *361−362*, 72−79.
(79) Drago, R. S.; Corden, B. B.; Barnes, C. W. Novel cobalt(II)-catalyzed oxidative cleavage of a carbon-carbon double bond. *J. Am. Chem. Soc.* **1986**, *108*, 2453−2454.
(80) The interstitial solvent in the crystals studied by SC-XRD will be often omitted throughout the text for clarity.
(81) Arion, V. B.; Simonov, Yu. A.; Gerbeleu, N. V.; Dvorkin, A. A.; Gradinaru, D. I.; Malinovskii, T. I. Template synthesis and structure of the pentacoordinate complex of cobalt(III) with 2,4-pentanedione bis(*S*-methylisothiosemicarbazone). *Dokl. Akad. Nauk SSSR* **1992**, *325*, 502−507.
(82) A thrice deprotonated ligand was documented in the iron(IV) complexes with PBIT, namely, $[Fe^{IV}(L^{Alk})I]$, where Alk = S-Alkyl.[S1,S2]
(83) Davies, S. C.; Durrant, M. C.; Hughes, D. L.; Pezeshk, A.; Richards, R. L. Coordination chemistry of a pyrazoline derived from 2,4-pentanedione bis(4-methylthiosemicarba-zone). Crystal structure of the pyrazoline and evidence for metal-mediated ring opening. *J. Chem. Res.* **2001**, *2001*, 100−103.
(84) Cowley, A. R.; Dilworth, J. R.; Donnelly, P. S.; Gee, A. D.; Heslop, J. M. Acetylacetonate bis(thiosemicarbazone) complexes of copper and nickel: towards new copper radiopharmaceuticals. *Dalton Trans.* **2004**, 2404−2412.
(85) Bilyj, J. K.; Riley, M. J.; Bernhardt, P. V. Isomerism and reactivity of nickel(II) acetylacetonate bis(thiosemicarbazone) complexes. *Dalton Trans.* **2018**, *47*, 2018−2030.
(86) Blanchard, S.; Neese, F.; Bothe, E.; Bill, E.; Weyhermüller, T.; Wieghardt, K. Square planar vs tetrahedral coordination in diamagnetic complexes of nickel(II) containing two bidentate π-radical monoanions. *Inorg. Chem.* **2005**, *44*, 3636−3656.
(87) Keilwerth, M.; Mao, W.; Jannuzzi, S. A. V.; Grunwald, L.; Heinemann, F. W.; Scheurer, A.; Sutter, J.; DeBeer, S.; Munz, D.; Meyer, K. From divalent to pentavalent iron imido complexes and an Fe(V) nitride via N−C bond cleavage. *J. Am. Chem. Soc.* **2023**, *145*, 873−887.
(88) Mao, W.; Fehn, D.; Heinemann, F. W.; Scheurer, A.; van Gastel, M.; Jannuzzi, S. A. V.; DeBeer, S.; Munz, D.; Meyer, K. Umpolung in a pair of cobalt(III) terminal imido/imidyl complexes. *Angew. Chem., Int. Ed.* **2022**, *61*, No. e202206848.
(89) Plenio, H.; Aberle, C.; Al Shihadeh, Y.; Lloris, J. M.; Martínez-Máñez, R.; Pardo, T.; Soto, J. Ferrocene−cyclam: a redox-active macrocycle for the complexation of transition metal ions and a study on the influence of the relative permittivity on the coulombic interaction between metal cations. *Chem. - Eur. J.* **2001**, *7*, 2848−2861.
(90) Lei, X.-W.; Yue, C.-Y.; Wei, J.-C.; Li, R.-Q.; Li, Y.; Mi, F.-Q. Transition metal complex directed lead bromides with tunable

https://doi.org/10.1021/jacsau.4c00005
JACS Au 2024, 4, 1166−1183

structures and visible light driven photocatalytic properties. *Dalton Trans.* **2016**, *45*, 19389−19398.
(91) Figgis, B.; Kucharski, E.; White, A. Crystal structure of bis(2,6-diacetylpyridine dihydrazone)cobalt(II) diiodide monohydrate. *Aust. J. Chem.* **1978**, *31*, 737−743.
(92) Linko, R. V.; Sokol, V. I.; Polyanskaya, N. A.; Ryabov, M. A.; Strashnov, P. V.; Davydov, V. V.; Sergienko, V. S. Molecular, crystal, and electronic structure of the cobalt(II) complex with 10-(2-benzothiazolylazo)-9-phenanthrol. *Crystallogr. Rep.* **2013**, *58*, 427−436.
(93) Jyai, R. N.; Srinivasan, B. R. Syntheses, structures, reactivity studies and properties of anionic water rich bivalent metal phthalates. *J. Mol. Struct.* **2019**, *1178*, 89−99.
(94) Klein Gebbink, R. J. M.; Jonas, R. T.; Goldsmith, C. R.; Stack, T. D. P. A periodic walk: a series of first-row transition metal complexes with the pentadentate ligand PY5. *Inorg. Chem.* **2002**, *41*, 4633−4641.
(95) Cariati, F.; Morazzoni, F.; Busetto, C.; Del Piero, G.; Zazzetta, A. Paramagnetic anisotropy in cobalt(II) Schiff-base complexes. X-ray crystal structure and electron spin resonance of NN′-ethylenebis(acetylacetoneiminato) cobalt(II)-doped NN′-ethylenebis(acetylacetone-iminato)nickel(II). *J. Chem. Soc., Dalton Trans.* **1976**, 342−347.
(96) Schaefer, W. P.; Marsh, R. E. Oxygen-carrying cobalt compounds. I. Bis(salicylaldehyde)ethylenediiminecobalt(II) monochloroformate. *Acta Crystallogr., Sect. B: Struct. Sci.* **1969**, *25*, 1675−1682.
(97) Whyte, A. M.; Shuku, Y.; Nichol, G. S.; Matsushita, M. M.; Awaga, K.; Robertson, N. Planar Ni(II), Cu(II) and Co(II) tetraaza[14]annulenes: structural, electronic and magnetic properties and application to field effect transistors. *J. Mater. Chem.* **2012**, *22*, 17967−17975.
(98) Zhang, R.-h.; Wang, Q.; Yang, G. Synthesis and crystal structures of the first cobalt complexes of macrocyclic oxamido. *Inorg. Chim. Acta* **2012**, *390*, 178−183.
(99) The Co−N bonds are shorter than those reported for a macrocyclic square-planar oxamido-cobalt(II) complex[96] varying from 1.9013(15) to 1.9168(17) Å.
(100) Weiss, M. C.; Bursten, B.; Peng, S.-M.; Goedken, V. L. Effects of peripheral steric constraints and metal ion size on the structure of three five-coordinate macrocyclic ligand complexes of the type $[M(C_{22}H_{22}N_4)X]$, M = cobalt(III), iron(III), manganese(II); X = iodine, chlorine, triethylamine. *J. Am. Chem. Soc.* **1976**, *98*, 8021−8031.
(101) Daikh, B. E.; Hutchison, J. E.; Gray, N. E.; Smith, B. L.; Weakley, T. J. R.; Finke, R. G. An unprecedented and reversible cobalt-to-carbon alkyl bond rearrangement in the coenzyme B12 model complex $C_6H_5CH_2Co^{III}$[C2(DO)(DOH)pn]I. *J. Am. Chem. Soc.* **1990**, *112*, 7830−7832.
(102) Leovac, V. M.; Herak, R.; Prelesnik, B.; Niketic, S. R. Transition metal complexes with thiosemicarbazide-based ligands. Part 13. Synthesis and structure of μ-oxo-bis-{[pentane-2,4-dione bis(*S*-methylisothiosemicarbazonato-κ^2 N,N″)(3−)]iron(IV)}. *J. Chem. Soc., Dalton Trans.* **1991**, 2295−2299.
(103) Further evidence for the oxidation state −1 for the tetradentate ligand in 3 is provided by the shortening of the N2−N3 bond and lengthening of the C1−N2 bond by 0.06 and 0.03 Å, respectively, compared to the average N−N bond and average C1−N2/C5−N5 bonds, respectively, in $[Co^{III}(H_2L^{SMe})I]I$.
(104) Westre, T. E.; Kennepohl, P.; DeWitt, J. G.; Hedman, B.; Hodgson, K. O.; Solomon, E. I. A Multiplet analysis of Fe K-edge 1s → 3d pre-edge features of iron complexes. *J. Am. Chem. Soc.* **1997**, *119*, 6297−6314.
(105) Chandrasekaran, P.; Chiang, K. P.; Nordlund, D.; Bergmann, U.; Holland, P. L.; DeBeer, S. Sensitivity of X-ray core spectroscopy to changes in metal ligation: a systematic study of low-coordinate, high-spin ferrous complexes. *Inorg. Chem.* **2013**, *52*, 6286−6298.
(106) Baker, M. L.; Mara, M. W.; Yan, J. J.; Hodgson, K. O.; Hedman, B.; Solomon, E. I. K- and L-edge X-ray absorption spectroscopy (XAS) and resonant inelastic X-ray scattering (RIXS) determination of differential orbital covalency (DOC) of transition metal sites. *Coord. Chem. Rev.* **2017**, *345*, 182−208.
(107) DeBeer George, S.; Petrenko, T.; Neese, F. Prediction of iron K-edge absorption spectra using time-dependent density functional theory. *J. Phys. Chem. A* **2008**, *112*, 12936−12943.
(108) Roemelt, M.; Beckwith, M. A.; Duboc, C.; Collomb, M.-N.; Neese, F.; DeBeer, S. Manganese K-edge X-ray absorption spectroscopy as a probe of the metal−ligand interactions in coordination compounds. *Inorg. Chem.* **2012**, *51*, 680−687.
(109) Neese, F. The ORCA program system. *Wiley Interdiscip. Rev.: Comput. Mol. Sci.* **2012**, *2*, 73−78.
(110) Neese, F. Software update: the ORCA program system, version 4.0. *Wiley Interdiscip. Rev.: Comput. Mol. Sci.* **2018**, *8*, No. e1327.
(111) Neese, F.; Wennmohs, F.; Becker, U.; Riplinger, C. The ORCA quantum chemistry program package. *J. Chem. Phys.* **2020**, *152*, No. 224108.
(112) Neese, F. Software update: The ORCA program system—version 5.0. *Wiley Interdiscip. Rev.: Comput. Mol. Sci.* **2022**, *12*, No. e1606.
(113) Plasser, F.; Wormit, M.; Dreuw, A. New tools for the systematic analysis and visualization of electronic excitations. I. Formalism. *J. Chem. Phys.* **2014**, *141*, No. 024106.
(114) Römelt, C.; Weyhermüller, T.; Wieghardt, K. Structural characteristics of redox-active pyridine-1,6-diimine complexes: Electronic structures and ligand oxidation levels. *Coord. Chem. Rev.* **2019**, *380*, 287−317.
(115) Brown, S. N. Metrical oxidation states of 2-amidophenoxide and catecholate ligands: structural signatures of metal−ligand π bonding in potentially noninnocent ligands. *Inorg. Chem.* **2012**, *51*, 1251−1260.
(116) Waser, J.; Gaspar, B.; Nambu, H.; Carreira, E. M. Hydrazines and azides via the metal-catalyzed hydrohydrazination and hydroazidation of olefins. *J. Am. Chem. Soc.* **2006**, *128*, 11693−11712.
(117) Waser, J.; Nambu, H.; Carreira, E. M. Cobalt-catalyzed hydroazidation of olefins: convenient access to alkyl azides. *J. Am. Chem. Soc.* **2005**, *127*, 8294−8295.
(118) Crossley, S. W. M.; Obradors, C.; Martinez, R. M.; Shenvi, R. A. Mn-, Fe-, and Co-catalyzed radical hydrofunctionalizations of olefins. *Chem. Rev.* **2016**, *116*, 8912−9000.
(119) Isayama, S.; Mukaiyama, T. A New method for preparation of alcohols from olefins with molecular oxygen and phenylsilane by the use of bis(acetylacetonato)cobalt(II). *Chem. Lett.* **1989**, *18*, 1071−1074.
(120) Similarly, complex **1** was found to be entirely inactive.
(121) Hamilton, D. E.; Drago, R. S.; Zombeck, A. Mechanistic studies on the cobalt(II) Schiff base catalyzed oxidation of olefins by O_2. *J. Am. Chem. Soc.* **1987**, *109*, 374−379.
(122) Meinwald, J.; Labana, S. S.; Chadha, M. S. Peracid reactions. III. The oxidation of bicyclo [2.2.1]heptadiene. *J. Am. Chem. Soc.* **1963**, *85*, 582−585.
(123) Lacy, D. C.; Roberts, G. M.; Peters, J. C. The cobalt hydride that never was: revisiting Schrauzer's "hydridocobaloxime". *J. Am. Chem. Soc.* **2015**, *137*, 4860−4864.
(124) Estes, D. P.; Grills, D. C.; Norton, J. R. The reaction of cobaloximes with hydrogen: products and thermodynamics. *J. Am. Chem. Soc.* **2014**, *136*, 17362−17365.
(125) Complex **3** was less suitable due to its scarce solubility in organic solvents, including methanol.
(126) Lo, J. C.; Kim, D.; Pan, C.-M.; Edwards, J. T.; Yabe, Y.; Gui, J.; Qin, T.; Gutiérrez, S.; Giacoboni, J.; Smith, M. W.; Holland, P. L.; Baran, P. S. Fe-catalyzed C−C bond construction from olefins via radicals. *J. Am. Chem. Soc.* **2017**, *139*, 2484−2503.
(127) Kobayashi, K.; Nakazawa, H. Research on inorganic activators of dibromo Co-terpyridine complex precatalyst for hydrosilylation. *Dalton Trans.* **2022**, *51*, 18685−18692.
(128) Skrodzki, M.; Zaranek, M.; Witomska, S.; Pawluc, P. Direct dehydrogenative coupling of alcohols with hydrosilanes promoted by sodium tri(*sec*-butyl)borohydride. *Catalysts* **2018**, *8*, 618.

https://doi.org/10.1021/jacsau.4c00005
JACS Au 2024, 4, 1166−1183

(129) Cramer, H. H.; Ye, S.; Neese, F.; Werlé, C.; Leitner, W. Cobalt-catalyzed hydrosilylation of carbon dioxide to the formic acid, formaldehyde, and methanol level—how to control the catalytic network? *JACS Au* **2021**, *1*, 2058−2069.
(130) Obradors, C.; Martinez, R. M.; Shenvi, R. A. Ph(i-PrO)SiH_2: an exceptional reductant for metal-catalyzed hydrogen atom transfers. *J. Am. Chem. Soc.* **2016**, *138*, 4962−4971.
(131) Voronova, E. D.; Golub, I. E.; Pavlov, A.; Belkova, N. V.; Filippov, O. A.; Epstein, L. M.; Shubina, E. S. Dichotomous Si−H bond activation by alkoxide and alcohol in base-catalyzed dehydrocoupling of silanes. *Inorg. Chem.* **2020**, *59*, 12240−12251.
(132) Heinekey, D. M.; van Roon, M. Dihydride complexes of the cobalt and iron group metals: an investigation of structure and dynamic behavior. *J. Am. Chem. Soc.* **1996**, *118*, 12134−12140.
(133) Marinescu, S. C.; Winkler, J. R.; Gray, H. B. Molecular mechanisms of cobalt-catalyzed hydrogen evolution. *Proc. Natl. Acad. Sci. U.S.A.* **2012**, *109*, 15127−15131.
(134) Bertini, I.; Luchinat, C.; Parigi, G. Magnetic susceptibility in paramagnetic NMR. *Prog. Nucl. Magn. Reson. Spectrosc.* **2002**, *40*, 249−273.
(135) Bertini, I.; Luchinat, C.; Parigi, G.; Ravera, E. The Hyperfine Shift. In *Solution NMR of Paramagnetic Molecules*, 2nd ed.; Bertini, I.; Luchinat, C.; Parigi, G.; Ravera, E. B., Eds.; Elsevier: Boston, 2017; pp 25−60.
(136) Tsitovich, P. B.; Cox, J. M.; Benedict, J. B.; Morrow, J. R. Six-coordinate iron(II) and cobalt(II) paraSHIFT agents for measuring temperature by magnetic resonance spectroscopy. *Inorg. Chem.* **2016**, *55*, 700−716.
(137) Ravera, E.; Gigli, L.; Czarniecki, B.; Lang, L.; Kümmerle, R.; Parigi, G.; Piccioli, M.; Neese, F.; Luchinat, C. A Quantum chemistry view on two archetypical paramagnetic pentacoordinate nickel(II) complexes offers a fresh look on their NMR spectra. *Inorg. Chem.* **2021**, *60*, 2068−2075.
(138) Blahut, J.; Benda, L.; Kotek, J.; Pintacuda, G.; Hermann, P. Paramagnetic cobalt(II) complexes with cyclam derivatives: toward ^{19}F MRI contrast agents. *Inorg. Chem.* **2020**, *59*, 10071−10082.
(139) Novitchi, G.; Riblet, F.; Helm, L.; Scopelliti, R.; Gulea, A.; Merbach, A. E. Richness of isomerism in labile octahedral Werner-type cobalt(II) complexes demonstrated by ^{19}F NMR spectroscopy: structure and stability. *Magn. Reson. Chem.* **2004**, *42*, 801−806.
(140) Riblet, F.; Novitchi, G.; Scopelliti, R.; Helm, L.; Gulea, A.; Merbach, A. E. Isomerization mechanisms of stereolabile *tris*- and *bis* -bidentate octahedral cobalt(II) complexes: X-ray structure and variable temperature and pressure NMR kinetic investigations. *Inorg. Chem.* **2010**, *49*, 4194−4211.
(141) Revenco, M. D.; Gerbeleu, N. V.; Simonov, Yu. A.; Bourosh, P. N.; Vyrtosu, N. I.; Sobolev, A. N.; Malinovskii, T. I. Synthesis and structure of cobalt(III) pentacoordinated compound based on S-methyl-1-phenylisothiosemicarbazide. *Dokl. Akad. Nauk SSSR* **1988**, *300*, 127−131.
(142) Blanchard, S.; Bill, E.; Weyhermüller, T.; Wieghardt, K. *N,N*-Coordinated π radical anions of *S*-methyl-1-phenyl-isothiosemicarbazide in two five-coordinate ferric complexes $[Fe^{III}(L^{Me\bullet})_2X]$ (X = CH_3S^-, Cl^-). *Inorg. Chem.* **2004**, *43*, 2324−2329.
(143) Revenco, M. D.; Vyrtosu, N. I.; Gerbeleu, N. V.; Simonov, Yu. A.; Bourosh, P. N.; Sobolev, A. N. Synthesis and structure of nickel coordination compounds with sulfur-substituted 1-phenylazothiocarboximides. *Zh. Neorg. Khim.* **1988**, *33*, 2353−2359.
(144) Small differences in the bond distances in the two ligands are due to the *cis*-arrangement of the two isothiosemicarbazide moieties that are now incorporated into a tetradentate *N,N,N,N*-ligand platform PBIT and the presence of electron-donating aliphatic groups of the reduced Hacac moiety in $[Co^{III}(L^{SMe\bullet\bullet})I]$ instead of electron-withdrawing Ph groups in the two *S*-methyl-1-phenyl-isothiosemicarbazide ligands in *trans*-$[Co^{III}(Q^{Me\bullet})_2I]$ (see Chart 2 of the main text).
(145) Weiss, M. C.; Goedken, V. L. Chemistry of the macrocyclic cobalt(II) complex, $[Co(C_{22}H_{22}N_4)]$. Reactions with halogens, molecular oxygen, alkynes, and nitriles. *J. Am. Chem. Soc.* **1976**, *98*, 3389−3392.
(146) Yokota, S.; Tachi, Y.; Itoh, S. Oxidative degradation of β-diketiminate ligand in copper(II) and zinc(II) complexes. *Inorg. Chem.* **2002**, *41* (6), 1342−1344.
(147) Scheuermann, M. L.; Luedtke, A. T.; Hanson, S. K.; Fekl, U.; Kaminsky, W.; Goldberg, K. I. Reactions of five-coordinate platinum(IV) complexes with molecular oxygen. *Organometallics* **2013**, *32*, 4752−4758.
(148) Kumar, P.; Lindeman, S. V.; Fiedler, A. T. Cobalt superoxo and alkylperoxo complexes derived from reaction of ring-cleaving dioxygenase models with O_2. *J. Am. Chem. Soc.* **2019**, *141*, 10984−10987.
(149) Kumar, P.; Devkota, L.; Casey, M. C.; Fischer, A. A.; Lindeman, S. V.; Fiedler, A. T. Reversible dioxygen binding to Co(II) complexes with noninnocent ligands. *Inorg. Chem.* **2022**, *61*, 16664−16677.
(150) Rodríguez-Lugo, R. E.; Trincado, M.; Vogt, M.; Tewes, F.; Santiso-Quinones, G.; Grützmacher, H. A Homogeneous transition metal complex for clean hydrogen production from methanol−water mixtures. *Nat. Chem.* **2013**, *5*, 342−347.
(151) Nadif, S. S.; O'Reilly, M. E.; Ghiviriga, I.; Abboud, K. A.; Veige, A. S. Remote multiproton storage within a pyrrolide-pincer-type ligand. *Angew. Chem., Int. Ed.* **2015**, *54*, 15138−15142.

https://doi.org/10.1021/jacsau.4c00005
JACS Au 2024, 4, 1166−1183